CHAPTER 5

EXPERIMENTAL RESULTS

5.1 Boresight Calibration

To compare the accuracy of determined boresight misalignment parameters, both the manual tie point selections and the tie points detected with image matching are applied in this research.

5.1.1 Manual tie point selection

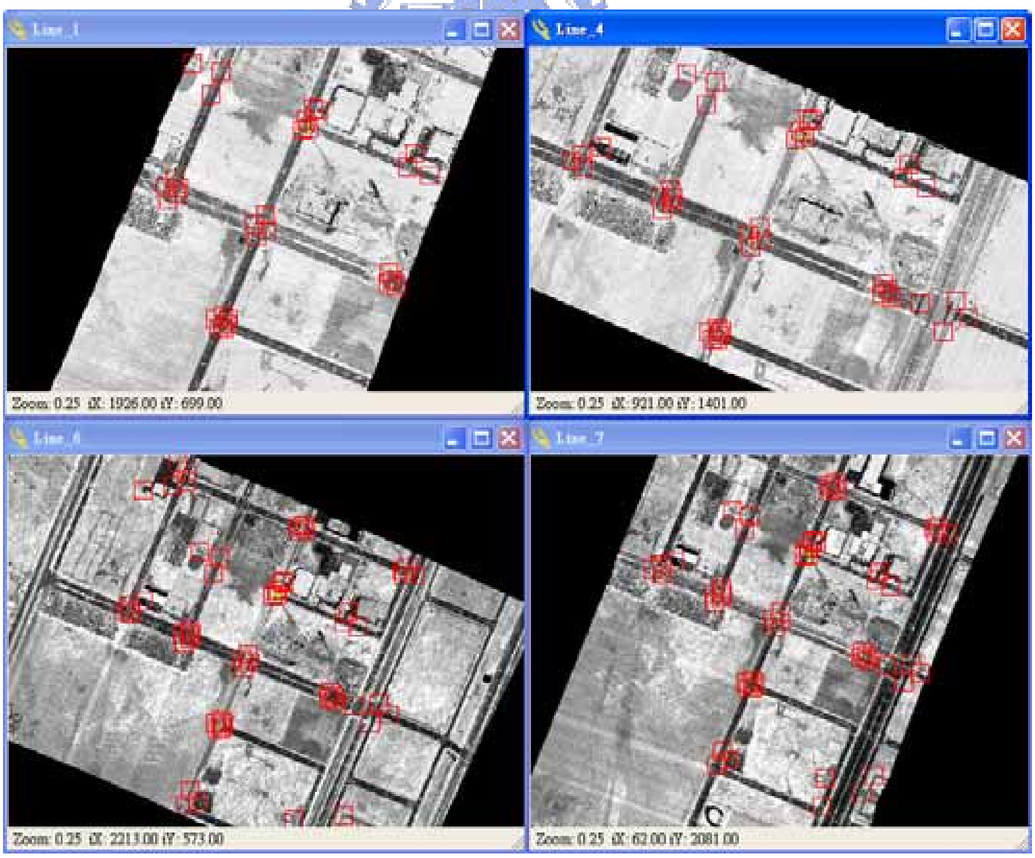

Figure 5.1: Manual selected tie point distribution

In this test a total of 58 points were selected as tie points. The tie point distribution is shown in Figure 5.1. Tie point that have large residuals are identified as outliers. The procedure allows for a quick identification and removal of points that have large residuals. The solution was repeated until no outliers remained. Among the 58 tie points, three outliers were rejected. The tie point differences and regular point elevation differences are affected by the large planimetric shifts between the uncalibrated strips. Thus, a grid point in one strip will generally not correspond to the same point in the second strip. The initial tie point differences are presented in Table 5.1.

Table 5.1: Initial tie point differences

	X (m)	Y (m)	Z (m)
Mean	26.269	25.232	6.522
Median	25.340	25.211	5.902
Minimum	25.210	24.877	4.908
Maximum	29.487	25.538	9.853
Std Dev	1.780	2.152	1.831

The most telling indication of calibration errors can be seen in the graphical profile plot. As shown in Figure 5.2a, discrepancies are plainly visible by plotting along structures such as buildings with peaked roofs. Figure 5.2a shows clear angular differences between the four overlapping strips, elevation offsets and planimetric shifts. What is not plain to see, however, is that the strips are not simply shifted from each other, but are distorted across all 3 dimensions. The significant discrepancies between calibration strips are caused by incorrect boresight angles (used 0, 0 and 0 as initial approximation in this test) on purpose, as was discussed.

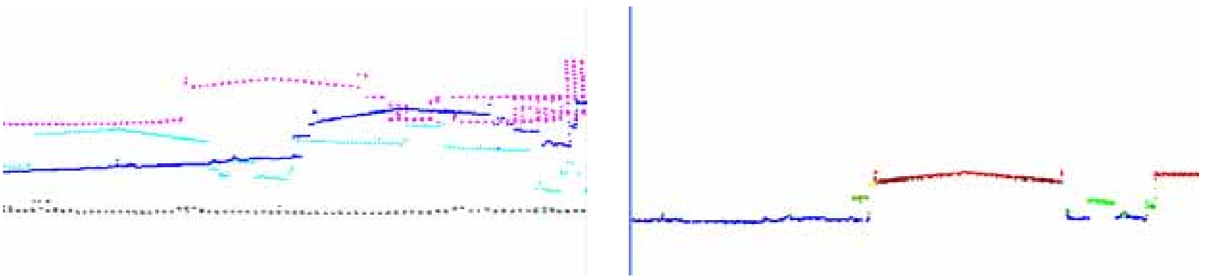

a. Before calibrated b. After calibrated

Figure 5.2: Profiles for uncalibrated and calibrated ALS strips

The calibrated tie point difference presented in Table 5.2 is now shown with the boresight calibration parameters in Table 5.3. In contrast to Table 5.2, the tie points show a much better alignment with an average planimetric difference of 0.60 m and an average elevation difference of 0.04 m. The planimetric error of the tie points of 0.60 m is a little higher than the expected value of 0.5 m, which is equivalent to the set weight while applying adjustment.

Table 5.2: Tie point differences after calibrated

	X (m)	Y (m)	Z (m)
Mean	0.585	0.616	0.040
Median	0.513	0.497	0.037
Minimum	0.154	0.171	0.008
Maximum	2.840	2.472	0.335
Std Dev	0.390	0.406	0.041

Table 5.3: Boresight parameters from manual tie point selection

Parameters	Value	Standard deviation	Standard deviation
Roll Error	-0.043961080 rad	0.00002062 rad	0.001181 degrees
Pitch Error	0.010520580 rad	0.00003020 rad	0.001730 degrees
Heading Error	-0.001312620 rad	0.00013519 rad	0.007746 degrees
Torsion	-10272.896 units	0.00007571311	0.00007571311

As presented in Table 5.3, the standard deviation of the roll error shows that the roll is the best-calibrated parameter. As the roll induces the largest elevation differences in the selected tie points, it has the largest chance to adjust – resulting in a more precise solution. Next, the standard deviation of pitch is a little larger than the roll, but much better than the IMU (*Applanix POS 501*) pitch error of 0.005 degrees. This suggests that ALS strip collected at a different altitude is successful in separating out the influence of pitch error.

Lastly, Table 5.3 also demonstrates that the heading error is the weakest component of the solution. The standard deviation of heading errors is almost five times larger than both the roll and the pitch. This can be explained by the dependency of the heading on the planimetric quality of the tie points (Figure 4.3). It can be concluded that the heading error would be the poorest-determined parameter. The standard deviation of heading errors, however, is a little smaller than the IMU heading error of 0.008 degrees. This implies that the solution can achieve a reasonable precision, no matter what the tie point selection is. For ease of communication, the computed boresight calibration parameters (Table 5.3) will be henceforth named as *Manual_cal* in the remaining parts of this research.

By re-calculating the point clouds in the mapping frame with the computed boresight calibration parameters in Table 5.3, the point clouds should fit the surface to which they belong. As shown in Figure 5.2b, the profile generated from four calibrated strips shows much better agreement.

Basically, the accuracy of manual tie point measurement should reach *ps*/3 (*ps* = pixel size) in digital photogrammetry. The intensity images used in the *Attune* program and the height/intensity images used in this dissertation are based on interpolated regular grid. Therefore, these images are much different from traditional photogrammetric images. Furthermore, the size of laser footprints varies with the strength of reflectance and the factors of terrain. If the interpolated grid size is set as 1.0 m and is assumed as the pixel size of images, the accuracy of tie point measurement should be less than 33 cm.

Table 5.4: The calibrated tie points difference from 3 operators

Operators	A			B			C		
X/Y/Z	X (m)	Y (m)	Z (m)	X (m)	Y (m)	Z (m)	X (m)	Y (m)	Z (m)
Mean	0.585	0.616	0.040	0.471	0.544	0.058	0.553	0.595	0.039
Median	0.513	0.497	0.037	0.427	0.560	0.041	0.479	0.551	0.041
Min.	0.154	0.171	0.008	0.096	0.146	0.008	0.108	0.156	0.008
Max.	2.840	2.472	0.335	2.187	1.907	0.434	1.476	1.797	0.390
Std Dev	0.390	0.406	0.041	0.344	0.361	0.078	0.378	0.339	0.054

In a practical test, 3 operators are assigned to measure the tie points on the same data sets to compute the boresight calibration parameters. As shown in Table 5.4, this level of accuracy is very difficult to reach while applying manual tie point selection. With the innate limitation of horizontal accuracy of ALS data, how to set up the standard of accuracy on the tie point measurement for ALS interpolated data will be another issue that requires further research.

Next, the grid size should also be taken into account while measuring the tie points in the *Attune* program. Two kinds of grid size are applied to measure the tie points. The calibrated tie point difference is shown in Table 5.5, and the boresight calibration parameters are shown in Table 5.6. Both Tables 5.5 and 5.6 show that the accuracy of tie point differences as well as the computed boresight angles with 0.5 m grid size is better than the accuracy with 1.0 m grid size.

Table 5.5: Tie point differences after calibrated with two kinds of grid size

Grid size	1.0 m			0.5 m		
X/Y/Z	X (m)	Y (m)	Z (m)	X (m)	Y (m)	Z (m)
Mean	0.585	0.616	0.040	0.533	0.538	0.034
Median	0.513	0.497	0.037	0.504	0.506	0.031
Minimum	0.154	0.171	0.008	0.232	0.105	0.007
Maximum	2.840	2.472	0.335	0.960	0.895	0.090
Std Dev	0.390	0.406	0.041	0.185	0.197	0.019

Table 5.6: Boresight parameters from manual tie point selection with two kinds of grid size

Grid size	Parameters	Value	Standard deviation	Standard deviation
1.0 m	Roll Error	-0.043961080 rad	0.00002062 rad	0.001181 degrees
	Pitch Error	0.010520580 rad	0.00003020 rad	0.001730 degrees
	Heading Error	-0.001312620 rad	0.00013519 rad	0.007746 degrees
	Torsion	-10272.896 units	17.65598 units	17.65598 units
0.5 m	Roll Error	-0.04392362 rad	0.00001756 rad	0.001006 degrees
	Pitch Error	0.01059669 rad	0.00002652 rad	0.001519 degrees
	Heading Error	-0.00119921 rad	0.00011071 rad	0.006343 degrees
	Torsion	32040.465 units	93.061371 units	93.061371 units

The interpolation with a smaller grid size results in a higher boresight accuracy based on the parameters considered. However, the laser points are not evenly distributed. The constructed image can sometimes make tie point selection difficult when a grid size that is smaller than the average density of laser points is applied (Figure 5.3). Behan (2000) concluded that an interpolation method based on a TIN of the original points with a grid size that relates as closely as possible to the point density at acquisition is found to give the best results.

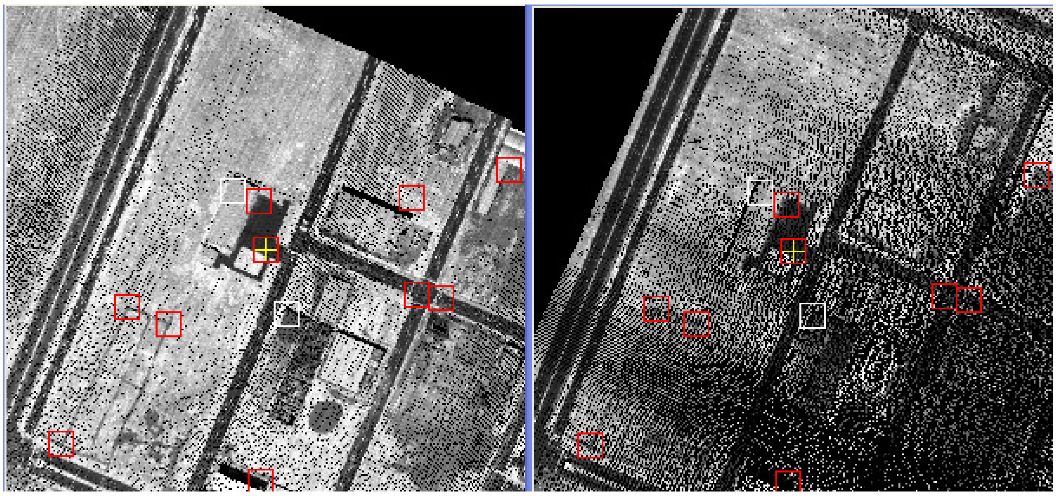

Figure 5.3: Intensity image with grid size smaller than average point density

It is clear that extreme care must be taken with the use of rasterized data for matching and the derivation of discrepancies between strips of laser data, particularly in terms of grid size and interpolation method.

5.1.2 Tie point detection with image matching

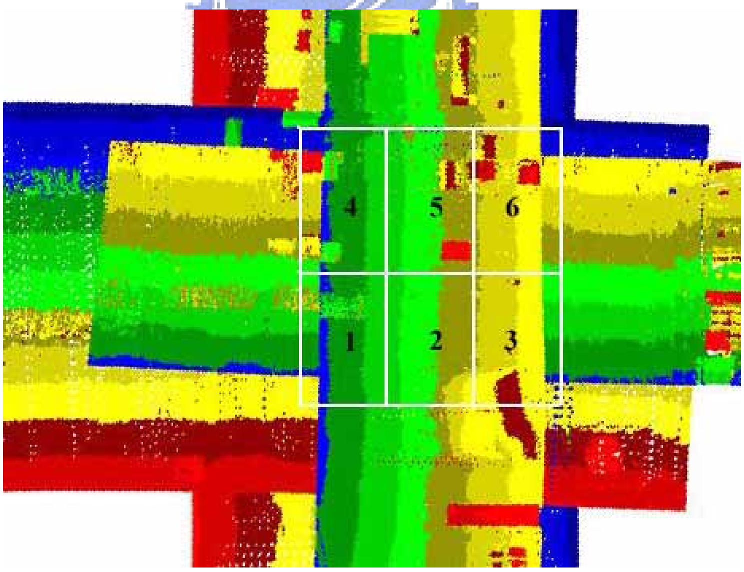

Figure 5.4: The location and extent of each patch

Both the height and intensity of uncalibrated ALS data, which were tested in Section 5.1.1, are used to examine the improvement on tie point selection, following the work flow (Figure 4.8). After preprocessing the strips data, each strip is split into six patches (Figure 5.4) in overlapping areas. Each patch is then interpolated to a grid with triangle-based linear interpolation (Figure 5.5).

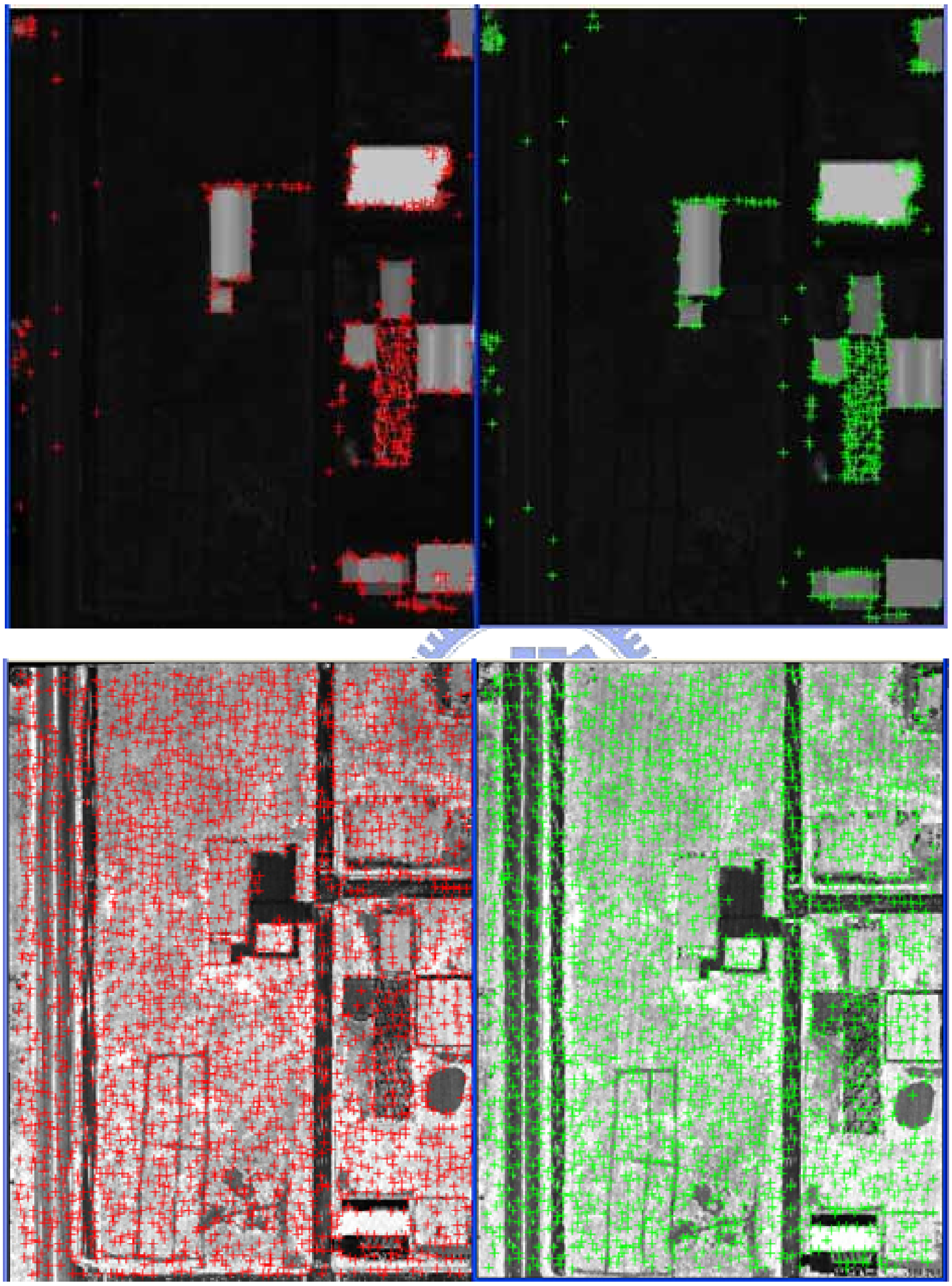

Figure 5.5: The detected interest points for the 4th patch in two strips

The triangulation with linear interpolation uses the optimal Delaunay triangulation (Watson, 1992; *MATHWORKS*, 2004). Triangulation with linear interpolation works best when the data are evenly distributed over the grid area. Therefore, the triangle-based linear interpolation is used for interpolating laser points since most of them are evenly distributed. The size of the grid was chosen to approximately correspond to the resolution of the laser points on the ground.

The automatic measurement of tie points generally requires two major steps. The first concerns the detection and the localization of interest points in images. Points of interest can be calculated individually from the images. Then these points are used to match the actual tie points. As was discussed in Section 4.1.4, Harris operator is used to detect the interest points for matching. The detected interest points are shown in Figure 5.5a and 5.5b for height and intensity data of the corresponding patches in two strips respectively.

Figure 5.5 immediately presents the significant difference of quantity on the detected interest points. This proves that the reflectance intensity of ALS can supply much more features as interest points than height data can. This is one of the critical factors for image matching. As presented in Figure 5.5a, the detected interest points from height data basically distribute on the corners of the buildings, the edges of the sidewalk and on the vegetation. It suggests that these areas have high variance of value (i.e. height value). Nevertheless, the detected interest points are evenly distributed throughout the whole image, as shown in Figure 5.5b.

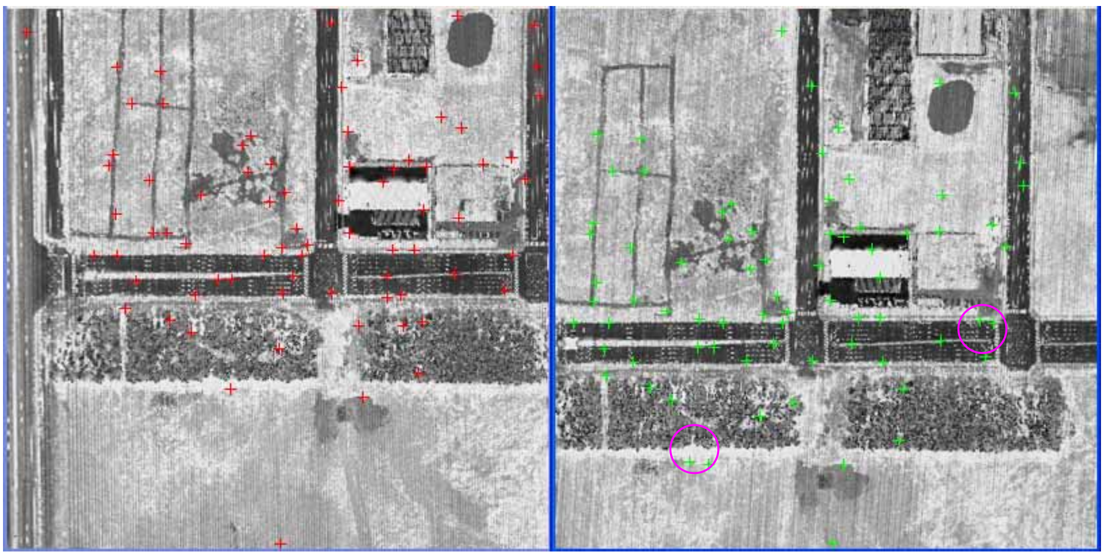

Figure 5.6: The detected interest points for the 4th patch in two strips

First, the intensity image is used for tie point detection. The matched tie points for the first patch are shown in Figure 5.6 based on an area-based matching technique. There are some incorrectly-matched points. For instance, one of the points in each circular zone (right image of Figure 5.6) doesn't appear on the image on the left hand side of Figure 5.6. These errors are mostly induced by the areas which are locally similar between two images (Figure 5.7). Two examples of correct points are shown in Figure 5.8.

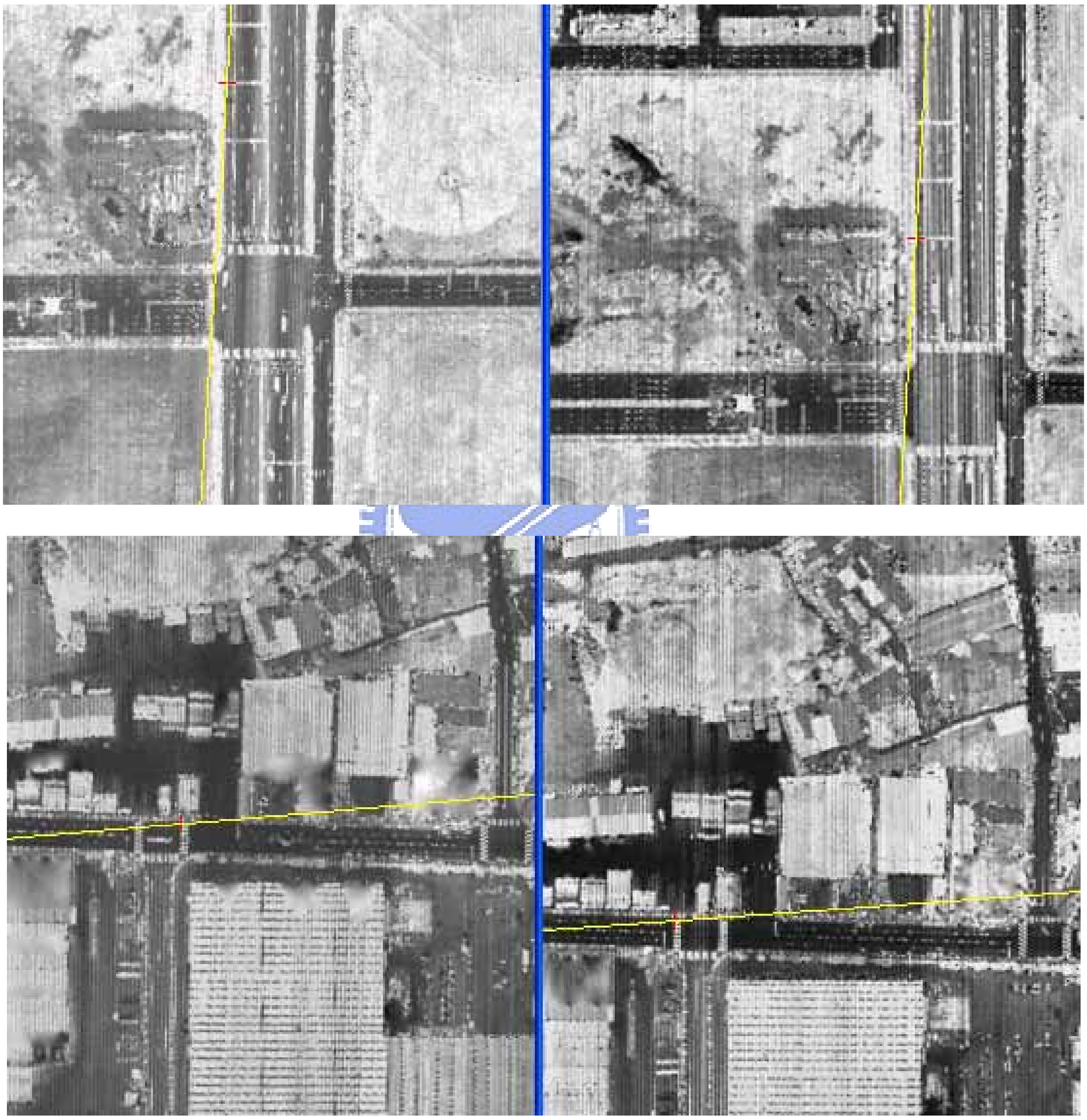

Figure 5.7: Examples of incorrect matching

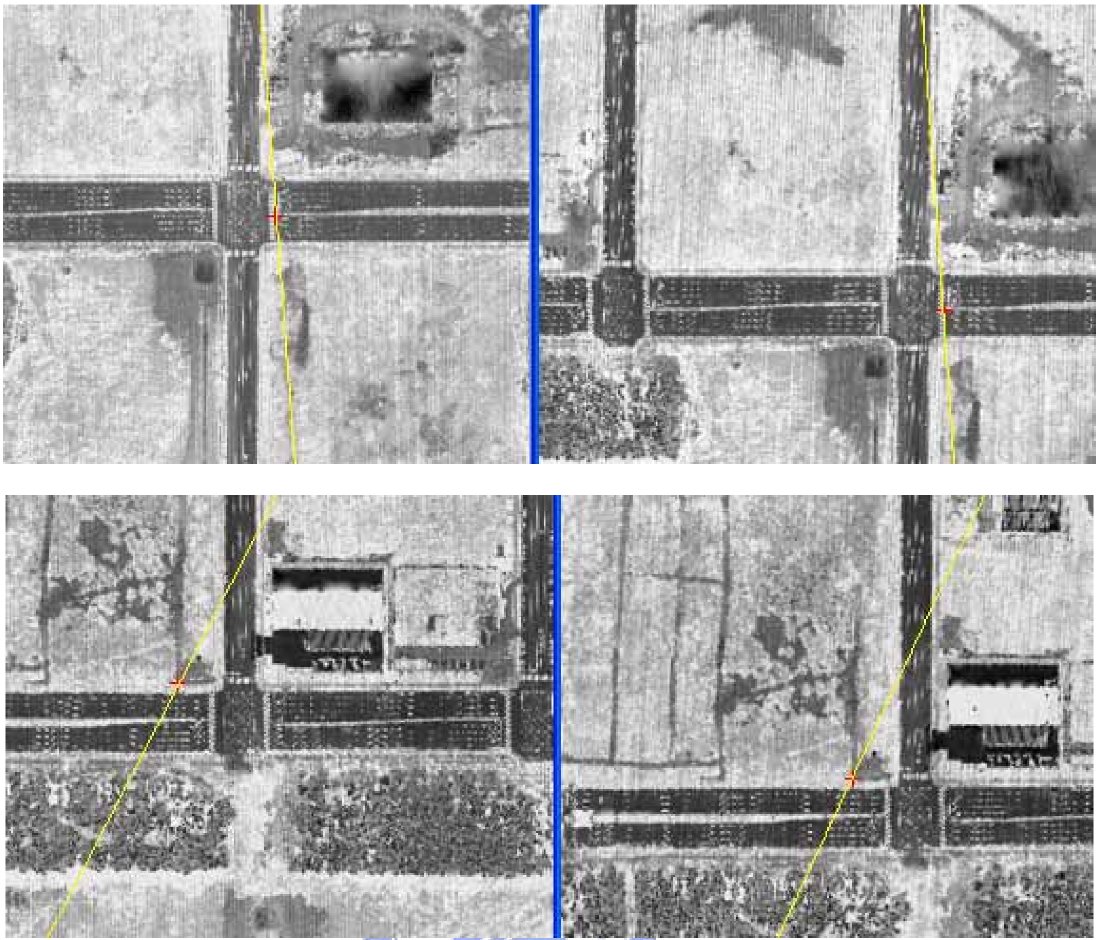

Figure 5.8: Examples of correct matching

The mentioned algorithm is applied to remove the incorrectly-matched points. All the correctly-matched points from the two overlapping ALS calibration strips after merging the six patches are shown in Figure 5.9. As expected, most of the successfully-matched points locate on the ground or on locally flat areas. This result is in accordance with one of the criteria for selecting tie points (section 4.1.3).

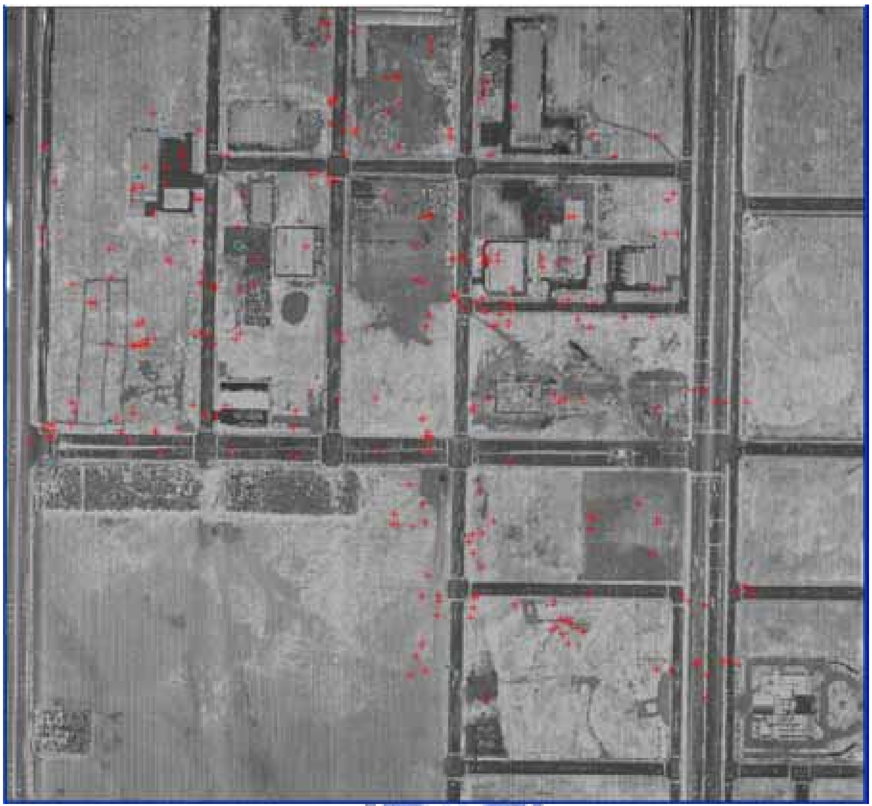

a. left

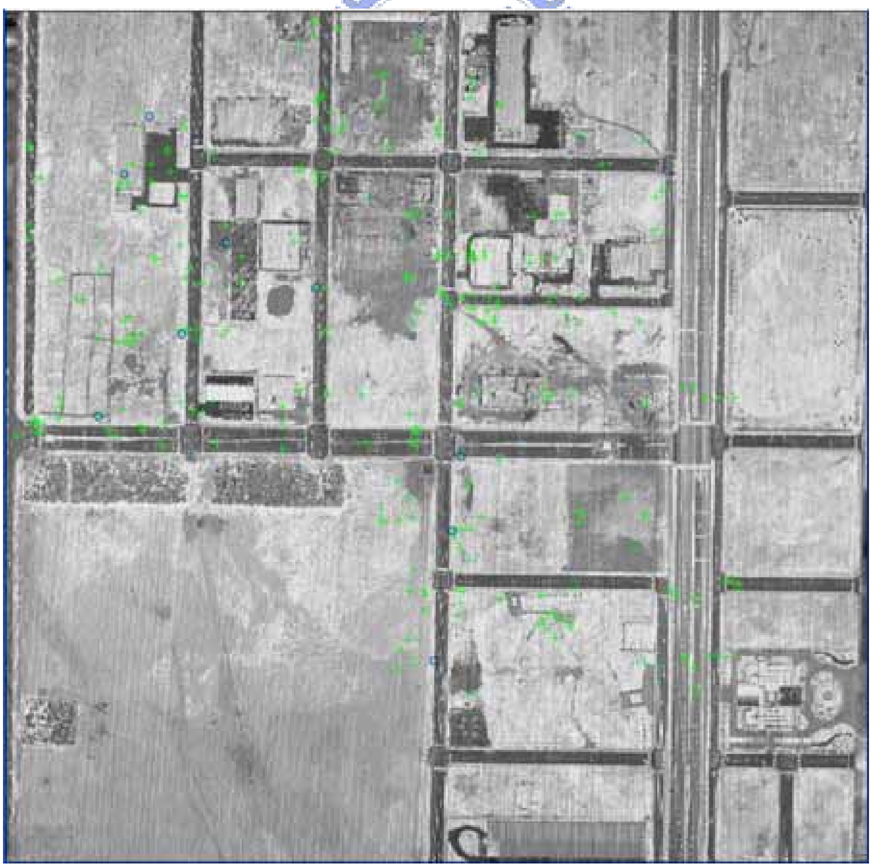

b. right

Figure 5.9: The matched points in two overlapping strips from intensity image

In addition to removing incorrectly-matched points, a visual assessment of the quality of tie points permits one to note that the percentage of erroneous tie points decreases appreciably with the order of the point (Kasser and Egels, 2002). The order of the point is defined as the number of images for which the point is visible. For example, the order of the point will reach four since there are four overlapping ALS strips used for boresight calibration in this research. There are several ways to exploit this observation with multiple points of order. A reliable method is to consider multiple point as valid if all associated measures are in total interconnection with regard to the similarity function, i.e. if each pair of measures is validated by image matching. As shown in Figure 5.10, every couple of points of this multiple link has been detected as pairs of homologous points by image matching.

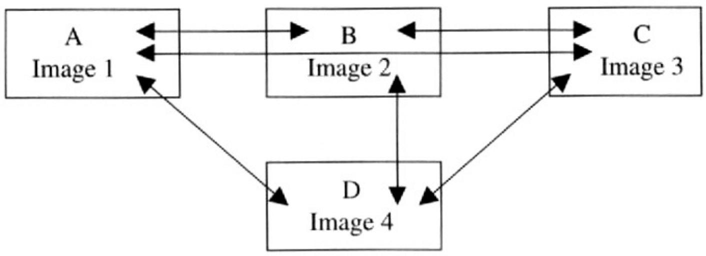

Figure 5.10: Multiple point of 4th order in total interconnection (Kasser and Egels, 2002)

Following the mechanism in Figure 5.10, there are six combinations of matching. To decrease the number of tie points that may be selected erroneously, a point has to appear on at least three images that are selected as final tie points to be employed in the adjustment procedure. The matched points with the third order (red cross in Figure 5.9a, green cross in Figure 5.9b) and the forth order (cyan circle in Figure 5.9a, blue circle in Figure 5.9b) are also shown in Figure 5.9.

The initial tie point differences and the calibrated tie point differences are depicted in Tables 5.7 and 5.8, respectively. Compared to Table 5.2, the tie point residuals in Table 5.7 show a significant improvement from this solution (with an average planimetric value of 0.28 m and an average elevation value of 4.5 cm). Moreover, the accuracy of tie points is much better than the previous solution (Table 5.2) (with a standard deviation of XY value dropping from 0.40 m to 0.15 m and Z value dropping from 4.1 cm to 2.3 cm).

Table 5.7: Initial tie point differences by using intensity images

	X (m)	Y (m)	Z (m)
Mean	43.992	33.867	8.380
Median	47.835	32.975	6.143
Minimum	31.982	32.526	2.291
Maximum	48.335	36.915	15.897
Std Dev	7.393	1.848	5.134

Table 5.8: Tie point differences after calibrated by using intensity images

	X (m)	Y (m)	Z (m)
Mean	0.274	0.283	0.045
Median	0.247	0.266	0.040
Minimum	0.023	0.004	0.006
Maximum	1.019	0.645	0.101
Std Dev	0.161	0.133	0.023

The question is thus whether the higher accuracy of tie point selection leads to a higher accuracy of solution on calibration parameters. The computed calibration parameters from tie point detection by using intensity image matching are shown in Table 5.9. Similarity, the calibration parameters (Table 5.9), will be henceforth named as *Auto_cal* in the remaining parts of this document. In addition, the torsion parameter, which is the difference of computed parameters between *Manual_cal* and *Auto_cal*, is negligible. The standard deviation of roll and pitch in *Auto_cal* is very close to the solution in *Manual_cal*. The heading error is still the weakest component of the solution.

Table 5.9: Boresight parameters from image matching with intensity images

Parameters	Value	Standard deviation	Standard deviation
Roll Error	-0.04392137 rad	0.00001934 rad	0.001108 degrees
Pitch Error	0.01052102 rad	0.00002619 rad	0.001501 degrees
Heading Error	-0.00115289 rad	0.00013320 rad	0.007632 degrees
Torsion	28946.016 units	0.0000778640	0.0000778640

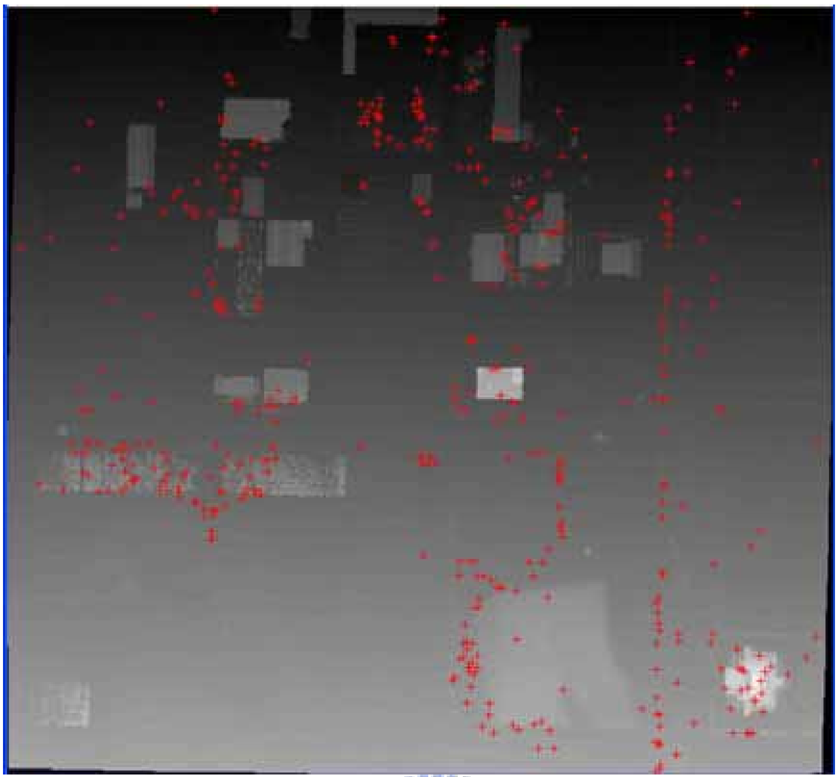

a. left

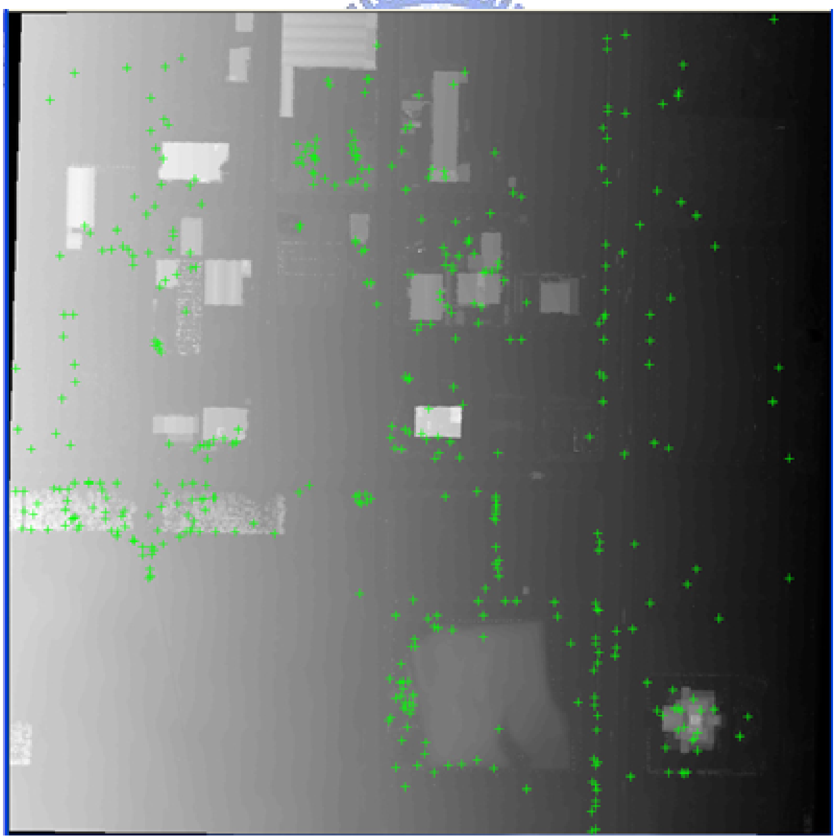

b. right

Figure 5.11: The matched points in two overlapping strips from height image

Higher accuracy of tie point selection did not lead to a higher accuracy solution of calibration parameters. In the end, it is up to the user to judge whether the boresight parameters calculated are "good enough". It is difficult to determine "what is good enough," nevertheless. In the next section, a popular measure by comparing laser points against ground check points will be applied to four validation strips to evaluate the boresight parameters.

For the sake of comparison, the height images derived from four quadrants of overlapping strips are also applied to image matching following the proposed workflow. An example of matched points from height image is shown in Figure 5.11.

Table 5.10: Initial tie point differences by using height images

	X (m)	Y (m)	Z (m)
Mean	47.825	32.774	11.968
Median	47.805	32.820	11.732
Minimum	47.619	32.582	8.116
Maximum	48.074	32.940	14.952
Std Dev	0.170	0.138	2.523

Table 5.11: Tie point differences after calibrated by using height images

	X (m)	Y (m)	Z (m)
Mean	0.276	0.296	0.597
Median	0.276	0.273	0.459
Minimum	0.031	0.020	0.008
Maximum	0.687	0.771	2.050
Std Dev	0.132	0.145	0.457

The initial tie point difference in height images is shown in Table 5.10, and the adjusted tie point residuals are presented in Table 5.11. The solution is in Table 5.12. Compared to the solution in *Manual_cal*, the tie point residuals in Table 5.11 also demonstrate a significant improvement on planimetry (with an average planimetric difference of 0.29 m and a standard deviation of planimetric value of 0.15 m).

However, both the average and the standard deviation of the height value are much worse than the solution in *Manual_cal* and *Auto_cal*. It suggests that most of the matched tie points from height images (distributed on bounds of roofs, the edges of sidewalk and on vegetation) will induce high elevation differences.

Finally, the accuracy of roll and pitch is worse than the solution in *Manual_cal* and *Auto_cal* resulting from larger height residuals of tie points. However, the accuracy is much better than the IMU roll/pitch error of 0.005 degrees. On the other hand, the accuracy of the heading error did not increase as expected and was larger than the IMU heading error of 0.008 degrees.

Table 5.12: Boresight parameters from image matching with height images

Parameters	Value	Standard deviation	Standard deviation
Roll Error	-0.04394853 rad	0.00003025 rad	0.001733 degrees
Pitch Error	0.01046488 rad	0.0000386 rad	0.002212 degrees
Heading Error	-0.00156200 rad	0.00024191 rad	0.013860 degrees
Torsion	9707.055 units*	0.00007571311	0.00007571311

5.1.3 Check by GCPs

There is no so-called "correct" boresight calibration parameter. To compare the accuracy of calibrated parameters between manual selection (*Manual_cal*) and selection with image matching (*Auto_cal*), 520 ground check points are used to estimate the height discrepancies. The evaluation of calibrated boresight parameters will not include the parameters which are used to derive the tie point with height image matching, (i.e. the parameter in Table 5.12), since the accuracy is much worse than the others.

The statistics of height differences between laser scanning points and known ground control are presented in Tables 5.13 and 5.14 for *Manual_cal* and *Auto_cal*, respectively. The computed height of point clouds by using *Manual_cal* is higher than check points with an average offsets from 1.7 cm to 5.2 cm. On the contrary, the computed elevation of points by applying *Auto_cal* is lower that check points with an average discrepancy from -4.6 cm to -1.3 cm. The standard deviation for both calibration parameters is in accordance with the vertical accuracy specifications of most commercial ALS systems (Leica, 2004a; Optech, 2004).

Table 5.13: Height differences from laser points against GCPs by applying *Manual_cal*

Strip No.	Average(m)	Std dev(m)	Minimum(m)	Maximum(m)	Points
1	0.052	0.038	-0.073	0.221	464
2	0.048	0.037	-0.062	0.171	462
3	0.017	0.050	-0.145	0.318	519
4	0.027	0.044	-0.127	0.191	516

Table 5.14: Height differences from laser points against GCPs by applying *Auto_cal*

Strip No.	Average(m)	Std dev(m)	Minimum(m)	Maximum(m)	Points
1	-0.013	0.039	-0.123	0.142	464
2	-0.019	0.035	-0.112	0.113	462
3	-0.046	0.049	-0.183	0.146	519
4	-0.038	0.042	-0.187	0.127	516

Significantly, the plotted profiles (Figure 5.12) generated from four ALS verifiable strips with the calibration parameters *Manual_cal* (Figure 5.12a) and *Auto_cal* (Figure 5.12b) applied show good alignments on a building roof. If the alignment of each of the flight line laser points does not appear to line up, it is necessary to repeat the adjustment by adding more tie points and/or refining the existing points.

a. Manual tie point selection

b. Tie point detection from intensity image matching

Figure 5.12: Profiles generated from calibrated ALS data

Once the average height differences have been taken from the four ALS strips, the last boresight misalignment parameter, i.e. the z (elevation) offset, can be derived. The ALS system elevation offset will always be the opposite of the determined value (Optech, 2003;

Leica, 2003a). This offset will shift the data in the opposite elevation direction to correct the laser point data to the known values.

To develop further understanding on the relationship between boresight parameters, correlation coefficients are calculated. A correlation coefficient is a numeric measure of the strength of a linear relationship between two random variables. The correlation matrix can be compiled from the adjustment report of the *Attune* program. A correlation matrix for each of *Manual_cal* and *Auto_cal* is shown in Tables 5.15 and 5.16, respectively. The correlation matrix based on tie point detection in height images is shown in Table 5.17 for the sake of comparison.

Table 5.15. The correlation matrix for *Manual_cal*

	Roll	Pitch	Heading	Torsion
Roll	1.000	0.014	-0.053	-0.090
Pitch	0.014	1.000	0.041	-0.097
Heading	-0.053	0.041	1.000	-0.004
Torsion	-0.090	-0.097	-0.004	1.000

Table 5.16. The correlation matrix for *Auto_cal*

	Roll	Pitch	Heading	Torsion
Roll	1.000	0.021	-0.058	-0.180
Pitch	0.021	1.000	-0.003	-0.106
Heading	-0.058	-0.003	1.000	-0.020
Torsion	-0.180	-0.106	-0.020	1.000

Table 5.17. The correlation matrix based on tie point detection by using height images

	Roll	Pitch	Heading	Torsion
Roll	1.000	0.027	-0.062	-0.100
Pitch	0.027	1.000	0.062	-0.114
Heading	-0.062	0.062	1.000	-0.002
Torsion	-0.100	-0.114	-0.002	1.000

The results presented in Tables 5.15, 5.16 and 5.17 show that the correlation between torsion/roll and torsion/pitch are much larger than the others.

Next, except the correlation of pitch/heading, the correlation of each parameter in *Manual_cal* (Table 5.15) is smaller than the correlation in *Auto_cal* (Table 5.16). It implies that the distribution of tie points correlate with the solution of misalignment parameter.

To conclude, the improvement on tie point selection in image-matching techniques for calibration presents a comparable accuracy against the techniques employed in manual measurements. The manual measurement of tie points is a time-consuming task, however. Previous experimental result reveals that any error in the tie point observation will degrade the calibration solution. The proposed automated method of extracting tie points can significantly upgrade the accuracy in tie point selection. Furthermore, an increased number of points would also provide more redundancy and improve the quality of the calibration parameters.

However, the automated method has a disadvantage, compared to the manual one. In the manual case, the operator can notably be assured of their geometric distribution a priori. In the automatic case, by contrast, the lack of intelligence of any computer method may be partly compensated by the abundance of data. Considering the distribution of points, it is difficult to force the machine to 'find' a solution in a given zone, and it is therefore probably preferable to let it find another solution in the neighborhood of the desired area.

5.1.4 Boresight Calibration for the Optech ALTM

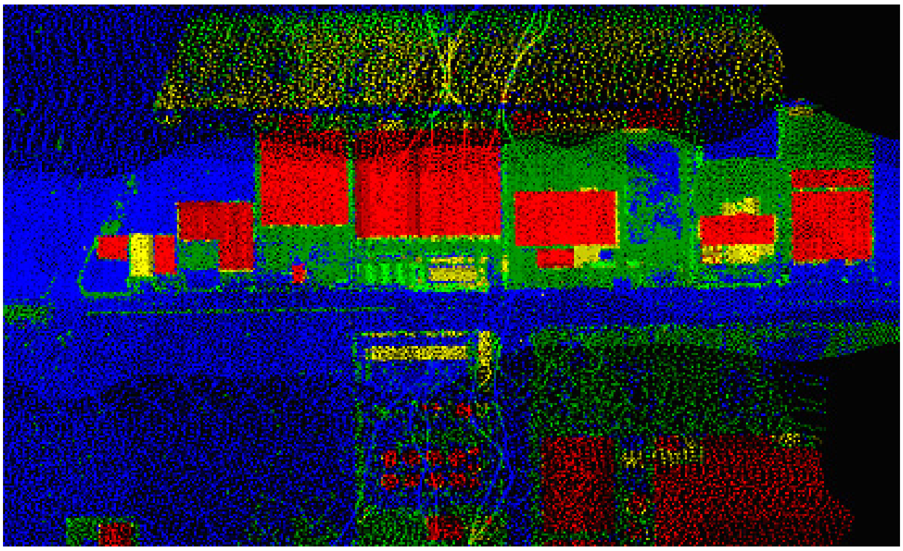

Figure 5.13: Boresight calibration data derived from the Optech ALTM 3070.

Following the schemes described in Section 4.1.5, a practical boresight calibration data set derived from the Optech ALTM is used in this section. Like the *Attune* used by the Leica system, the *Auto Calibrator* (*ACalib*) software is currently used for boresight calibration by the Optech system. Next, the calibration test data (Figure 5.13) derived from the Optech ALTM 3070 are used in processing the boresight calibration along with *ACalib*. The flight parameters are specified in Table 5.18.

Table 5.18: Flight parameters of boresight calibration for the Optech ALTM

Parameter	Value
Pulse rate	70 kHz
Scan rate	0/20/50 Hz
Returns/intensities	2/2
Operating altitude (AGL)	800 m
FOV	0/25/25 degree
Aircraft speed	125 knots

The computed boresight calibration parameters are presented in Table 5.19. The initial value in the Table 5.19 is the calibrated value performed in the laboratory. The computed boresight calibration parameters, i.e. the finial iterated value in Table 5.19, are very close to the value that was reported in a survey (CHSurvey, 2005).

Table 5.19: Boresight parameters from the Optech ALTM

Parameters	Initial value	The 1st iterated value	The final iterated value
Pitch	-0.017 degrees	-0.0297 degrees	-0.0707 degrees
Roll	-0.052 degrees	-0.0514 degrees	0.1411 degrees
Heading*	0.250 degrees	0.250 degrees	0.250 degrees
Scale	1.016398	1.008171	1.0008
TIMs	-2.658 m	-2.552 m	-2.552 m

* The heading value is not included for boresight calibration in the Optech ALTM.

The next step in processing the calibration data set is to analyze how well laser strips match each other. One way is to use different colors in the strips to differentiate between elevations. As shown in Figure 5.14, the color of each point shows how much the point exceeds or falls short of the average elevation of the overlapping strips at that location.

Yellow and green colors are less than 0.08 m from the average surface. Most of the points displayed in yellow or green indicate that the strips match each other pretty well. Additionally, the Figure 5.14b also suggests that the calibrated laser points of the overlapping strips match well with the profile of the roof of a building.

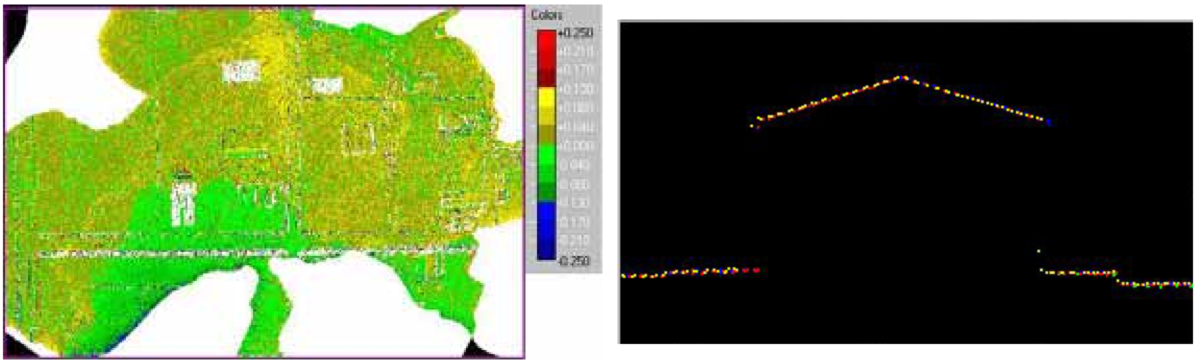

a. distance coloring　　　　　　　　　　b. building profile

Figure 5.14: Elevation differences coloring and building profile for Optech test data

Table 5.20: Height differences from calibrated laser points against GCPs for Optech data

	Average(m)	Std dev(m)	Minimum(m)	Maximum(m)	Points
For Optech	0.029	0.046	-0.092	0.671	1004

Correspondingly, 1004 ground check points are used to estimate the height discrepancy to evaluate the accuracy of the computed boresight parameters for Optech data. As depicted in Table 5.20, the standard deviation of the computed parameters meets the vertical accuracy requirement of the Optech ALTM. The elevation offset is therefore derived with 0.029 m from Table 5.20.

The schemes on boresight calibration for both the Leica ALS and the Optech ALTM are presented in this research. Because the current schemes on the boresight calibration are different for Leica and Optech, it is not possible to apply the Leica boresight calibration data to Optech boresight calibration scheme, and vice versa.

5.1.5 *TerraMatch*

To evaluate the accuracy of the misalignment parameters derived from the *Attune* program in Section 5.1.2, the *TerraMatch* program is also used to solve the misalignment parameters. Unlike the *Attune* program, the *TerraMatch* program needs an initial approximation of misalignment angles to access the laser point clouds. The computed misalignment parameters are shown in Table 5.3. The initial misalignment angles are given in Table 5.21. These angles are applied to the same ALS calibration flights data (Figure 4.14).

Table 5.21: The initial misalignment angles for *TerraMatch*

Parameters	Value
Roll Error	-0.042 rad
Pitch Error	0.009 rad
Heading Error	-0.001 rad

Table 5.22: Boresight misalignment angles from TerraMatch

Parameters	Value	Standard deviation
Roll Error	-0.0431711 rad	0.0002 degrees
Pitch Error	0.0104870 rad	0.0009 degrees
Heading Error	-0.0010506 rad	0.0006 degrees

As shown in Figure 5.15a, the height and planimetric discrepancies are present when the initial misalignment angles are applied. The computed misalignment angles and the corresponding standard deviation are depicted in Table 5.22. The standard deviation of the roll parameter shows that roll is the best-calibrated parameter, once again. The accuracy of the misalignment parameters is much better than the IMU error (with 0.005 degrees for roll/pitch, 0.008 degrees for heading). This implies that the solution is acceptable. Re-calculating the point clouds with the updated boresight calibration parameters leads to the profile shown in Figure 5.15b. The one that is generated from four calibrated strips shows much better agreement.

a. before calibrated b. after calibrated

Figure 5.15: Profiles of the building before and after calibrated of misalignment parameters

Table 5.23: Height differences from laser points against GCPs

	Average(m)	Std dev(m)	Minimum(m)	Maximum(m)	Points
Before correction	-0.077	0.166	-0.511	0.636	464
After correction	-0.037	0.037	-0.167	0.090	464

Correspondingly, 520 ground check points are used to estimate the height discrepancy in evaluating the accuracy of the computed misalignment parameters. The statistics of the height differences between laser scanning points and known ground control are presented in Table 5.23. The standard deviation for the computed parameters is also in accordance with the vertical accuracy specifications of most commercial ALS systems. The elevation offset is therefore derived with 0.037 m from Table 5.23.

Compared to *Attune, TerraMatch* is more sensitive with respect to the initial approximation of misalignment parameters. The process of adjustment is sometimes unable to converge or in need of a larger number of iterations to converge. It is empirically determined that the initial approximation for *TerraMatch* is a reasonable value provided by system vendors.

5.2 Systematic error validation

Next, the surface registration technique, that is, the ICP algorithm, is applied to measure the quantity of systematic errors. The goal of this experiment is to quantify the planimetry and the height offsets from the overlapping strip data. The transformed data surface (P) is the output file when the registration is carried out. Then the offsets in *X*-, *Y*-, and *Z*- directions between the overlapping strips can be derived after calculating the differences between the original and the transformed data surfaces.

A *MATLAB* code is used to implement the iterative closest point algorithm in this research. This program registers two data sets which are derived from airborne LiDAR. It is assumed that these two data sets are in approximation registration. These two data sets can be regarded as in approximation registration since they are extracted from two overlapping laser strips and are spread in the nadir zones in rough. Based on the equations and the computing steps presented in section 4.2, the code iterates until no more correspondence can be found. Two times the average distance between two laser points is used as the initial distance to establish correspondences. For instance, 1.0 m is used for test *I* and *II*. Finally, the threshold (τ) for iteration convergence is set as 0.00005 (*the average point distance/10000*).

5.2.1 Test Site I (*SI*)

The data sets with naturally existing systematic errors, like test data I (*SI*), are suitable for analyzing the performance of the proposed accuracy assessment procedure. To verify the systematic errors in strips 9 and 10, these two strips and their neighboring strips (strips 8 and 11) are selected as test data in this study (Figure 5.16). The eight patches are shown in Figure 5.16. The size of all patches is larger than 300 m × 300 m.

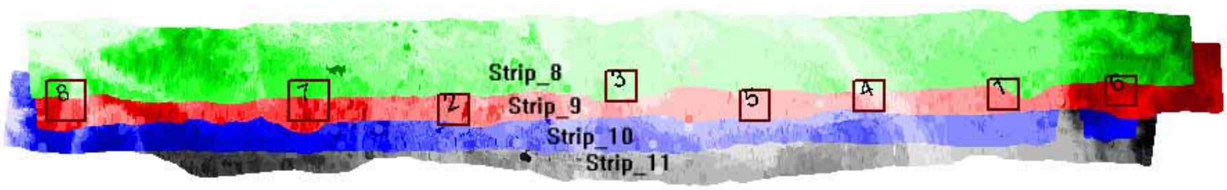

Figure 5.16: Four overlapping laser scanning strips in test site I (*SI*)

Due to the different width of laser scanning swath and irregular strip shape of ground coverage, the number of points falling into each patch varies between strips. The average height and its corresponding standard deviation for each patch are presented in Table 5.24. Larger average height differences are related to smaller overlapping percentage, and the presence of vegetation, or buildings (resulted in higher standard deviation). Patch-6 between strips 10 and 11 and patch-8 between strips 8 and 9 shown in Table 5.24 are two examples. Because the overlapping percentage between strips 8 and 11 is relatively small, the amount of common points of these two strips in these patches is smaller.

Table 5.24: The average height (μ, meters) and its standard deviation (σ, meters) in *SI*

Patches No.	Strip 8		Strip 9		Strip 10		Strip 11	
	μ	σ	μ	σ	M	σ	μ	σ
1	72.32	3.29	72.93	3.35	74.21	3.27	74.01	3.09
2	N/A*		75.40	11.04	76.66	10.64	76.58	10.70
3	54.58	3.10	54.46	2.96	56.06	2.69	N/A*	
4	51.72	3.77	55.81	6.74	55.25	7.02	58.90	7.10
5	N/A*		56.94	1.98	58.61	2.21	59.48	2.81
6	118.72	6.55	121.53	12.10	124.71	12.20	118.16	8.41
7	88.75	6.23	92.85	10.66	92.82	10.08	97.18	11.88
8	71.80	17.13	82.22	19.31	80.31	19.39	70.43	14.43

* There is no point falling into the overlapping area.

In order to examine the influence of surface type on the parameter of ICP algorithm, 8 experimental patches are selected based on various land use/land cover (LU/LC) categories. As discussed, some researchers (Crombaghs et al, 2000; Maas, 2003) use flat areas to estimate the height discrepancies to avoid the interpolating errors or to reduce the effect of terrain slope. It is found that the tolerance of iteration convergence of the ICP algorithm will need to be adjusted based on surface types, especially on flat areas.

The results of the analysis on 4 overlapping strips are summarized in Table 5.25. The amplitude of the height offsets is from -1.53 m to -1.80m with an average height offsets on the order of -1.67m for strips 9 and 10. Nevertheless, the height offsets are from -0.04 m to 0.19 m for strips 8 & 9 and strips 10 & 11 with an average difference on the order of 0.3 m. Based on Figure 4.11 and Table 5.25, it can be concluded that the significant height offsets exist among strips 10 to 19.

The average planimetric strip shifts range from -0.08 m to 0.204 m, as Table 5.25 shows, accompanying the planimetric shifts up to 0.60 m. Compared to the detected height offsets, the planimetric shifts are reasonable within the accuracy specifications defined in main commercial systems (Leica 2002; Optech 2002).

Table 5.25: Planimetry/height offset, applied to 8 patches of strip-8, 9, 10, and 11 for *SI*

Strips	8_9			9_10			10_11		
No. of patches	6			8			7		
Planimetry/Height	X	Y	Z	X	Y	Z	X	Y	Z
Average (m)	-0.07	0.08	0.033	0.008	-0.08	-1.667	0.204	-0.062	-0.029
Std dev (m)	0.014	0.04	0.016	0.047	0.051	0.03	0.047	0.075	0.018
Min. (m)	-0.359	-0.055	-0.037	-0.363	-0.401	-1.799	-0.108	-0.511	-0.067
Max. (m)	0.356	0.433	0.097	0.376	0.351	-1.532	0.606	0.187	0.187

Comparable transect elevations based on a building were plotted from the DSMs that are generated from 3 overlapping strips (strips 9, 10, and 11), as shown in Figures 5.17 and 5.18. The coordinates of x-axis in Figures 5.17 and 5.18 are the direction of the flight and the direction perpendicular to the flight, respectively. That is, Figure 5.17 has the x-axis in the along-track direction and Figure 5.18 has the x-axis in the across-track direction.

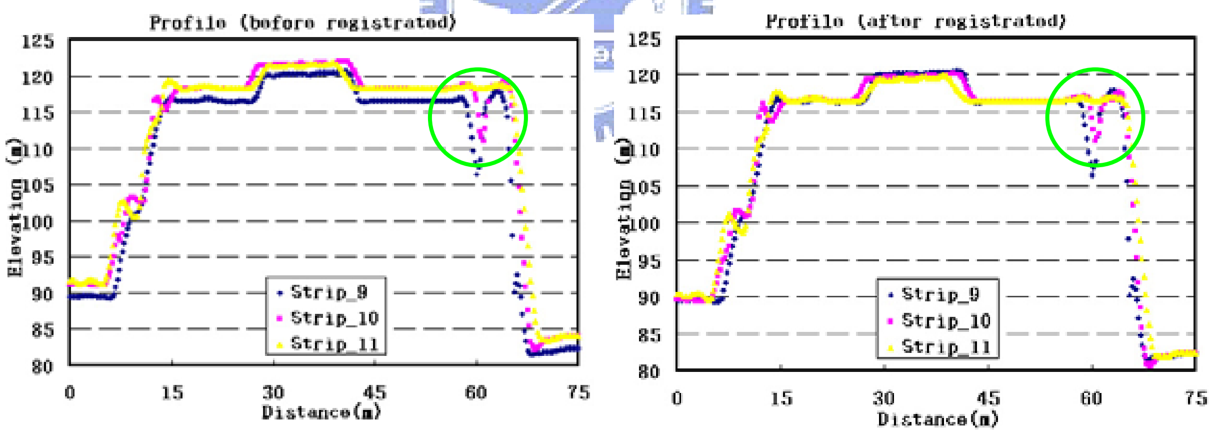

a. Profile from original data b. Profile from data with the ICP matching

Figure 5.17: Along-track profile comparison from 3 overlapping strips for *SI*

Figures 5.17a and 5.18a show significant height offsets both between strips 9 and 10, and between strips 9 and 11. The profiles produced from the data of registering all strips to strip 9 by the ICP display much better alignment (Figures 5.17b and 5.18b). Based on Table 5.25,

Figure 5.17, and Figure 5.18, it can be concluded that the surface registration with the ICP can sufficiently estimate the height offsets and planimetric shifts from overlapping laser scanning strips.

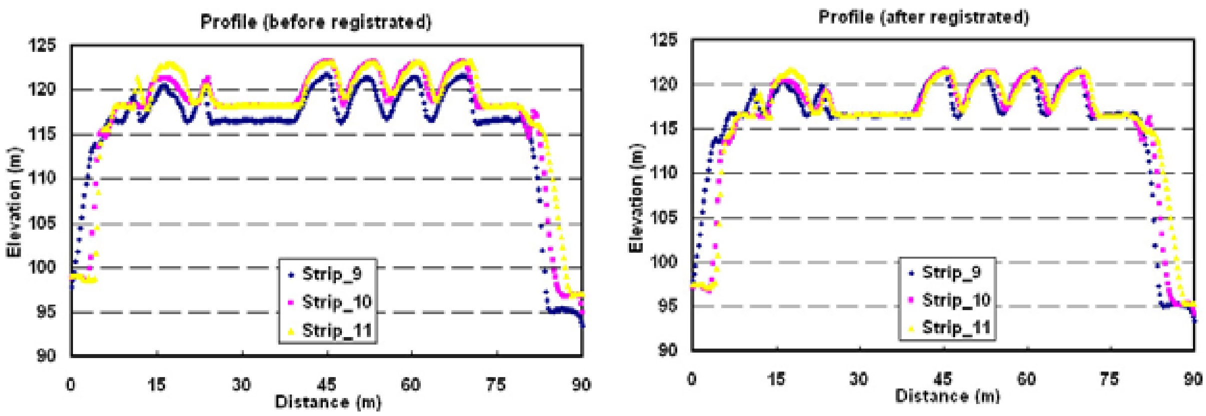

a. Profile from original data b. Profile from data with the ICP matching

Figure 5.18: Across-track profile comparison from 3 overlapping strips for *SI*

Figures 5.17 and 5.18 also reveal the along-track and across-track discrepancies among 3 adjacent strips. Furthermore, the recovery of systematic biases does not seem to be good enough based on the ICP algorithm, especially on the walls of this building which introduced occlusions. A severe problem when applying surface matching to patches containing roofs/walls is caused by occlusions typically occurring at one side of a building in one strip as a consequence of the quasi central perspective geometry of laser scanning in the across-flight direction (Maas, 2002). These occlusions become visible as gaps in one of the patches. Due to the composition of laser scanning data blocks of parallel strips, these occlusions will often occur in only one of the patches to be matched. For instance, the profile of strip-11 shows the occlusion effect in the circular zone in Figure 5.17. The analysis of the height data and the strip geometry suggests that the areas that were occluded in one strip are excluded from the matching (Kilian et al., 1996; Maas, 2002).

Figure 5.19 shows the trend of the planimetry shifts and height offsets for the first patch of 4 adjacent strips. The first row of Figure 5.19 shows that the x-shift (pitch induced) varies with the laser scanning patterns. The second row of Figure 5.19 reveals that the y-shift (roll induced) increases along the direction of flight for all strips. The last row of Figures 5.19a and

5.19c depicts the height offsets increasing toward the rim of the scanning extent in the across-track direction. The effects are induced by an oscillating scanner.

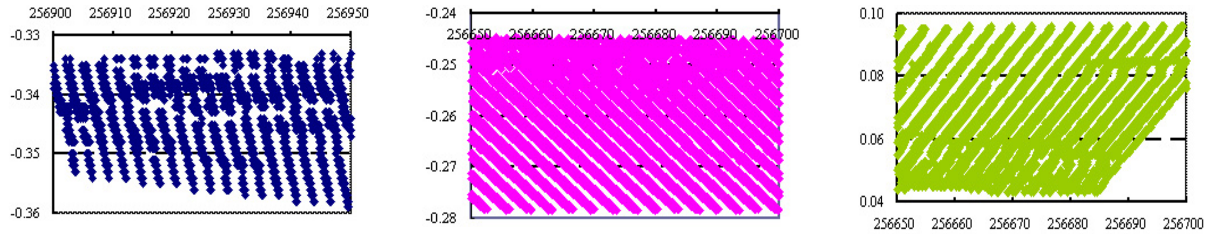

X coordinates vs. X-shift (m) X coordinates vs. X-shift (m) X coordinates vs. X-shift (m)

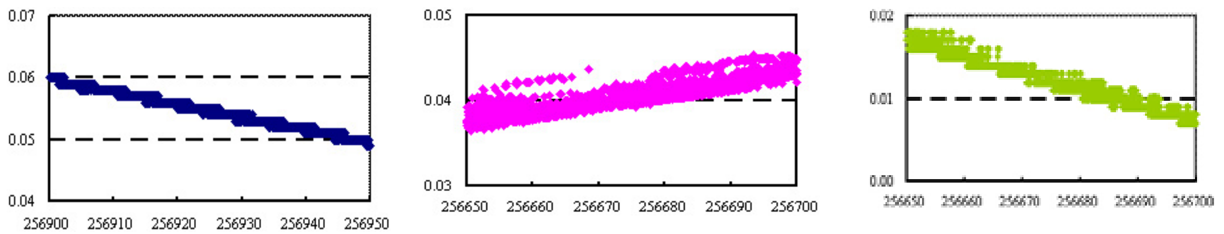

X coordinates vs. Y-shift (m) X coordinates vs. Y-shift (m) X coordinates vs. Y-shift (m)

Flight direction: E.←W. Flight direction: E.→ W. Flight direction: E.←W.

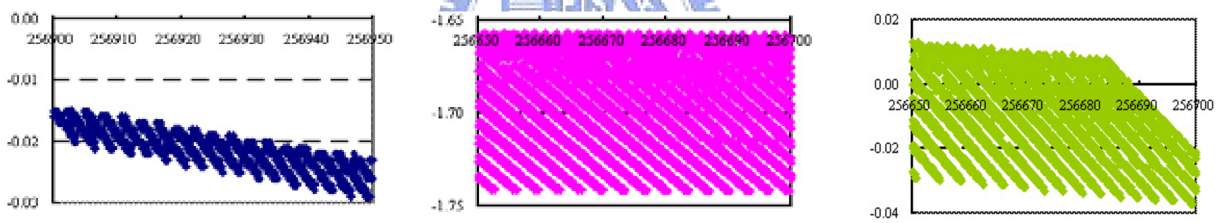

X coordinates vs. Z-offset (m) X coordinates vs. Z-offset (m) X coordinates vs. Z-offset (m)

a. Strip 8/9 b. Strip 9/10 c. Strip 10/11

Figure 5.19: Trend of planimetry/height shifts for patch- 1 in *SI*

Due to the limitation of the laser scanner's angular resolution, the elevation accuracy is usually much higher than the horizontal accuracy for ALS systems (Leica 2002; Optech 2002). With the height offsets much larger than the planimetry shifts, it implies that the systematic errors may be introduced by range biases or may come from an incomplete calibration between GPS and IMU frames. Regarding the height offsets between strips 1 to 9 and strips 10 to 19, the fact that the data are acquired in different dates may also play a role.

In order to achieve a higher density of laser scanning data to create good quality DSM, integrating all overlapping strips data is necessary. As shown in Figure 5.20a, the DSM (Golden Software, 1997) created from 4 original neighboring strips delineates the rugged surface due to the height offsets in some strips. On the contrary, Figure 5.20b presents a distinct DSM that integrated the 4 adjacent strips after the ICP matching algorithm is applied to the patches from strips 8, 10, and 11 with the patch of strip 9 fixed.

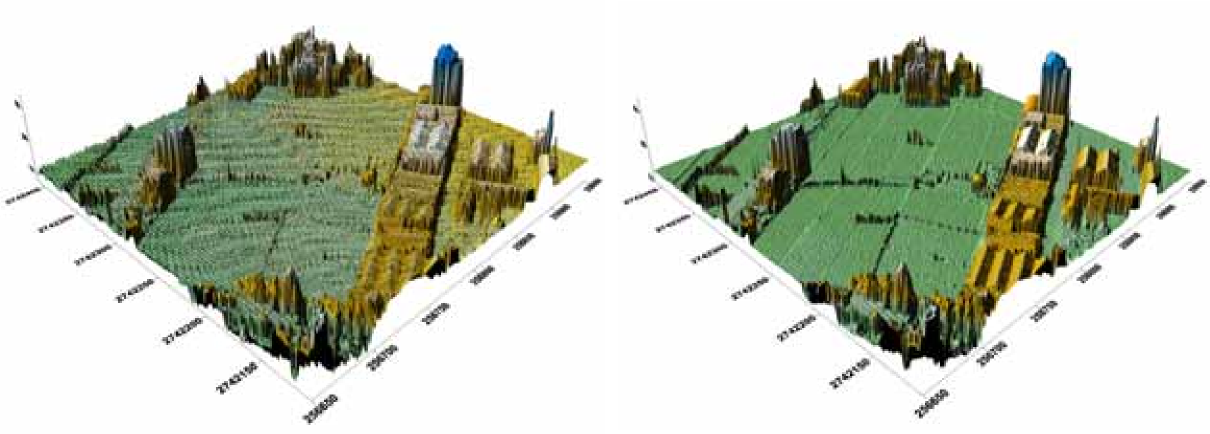

a. From original data. b. From data after the ICP matching when the patch of strip 9 is fixed.

Figure 5.20: DSM of the integrating 4 overlapping strips of patch 1 in *SI*

The texture shown in Figure 5.20 provides some useful information about the shape, orientation, and depth of objects. The human visual system employs texture as a visual cue for object recognition and image interpretation (Schenk, 1999). It can be easily found that the DSM in Figure 5.20b presents much more detailed texture than Figure 5.20a did, especially the ditches between rice paddies and the roofs of buildings.

5.2.2 Test Site II (*SII*)

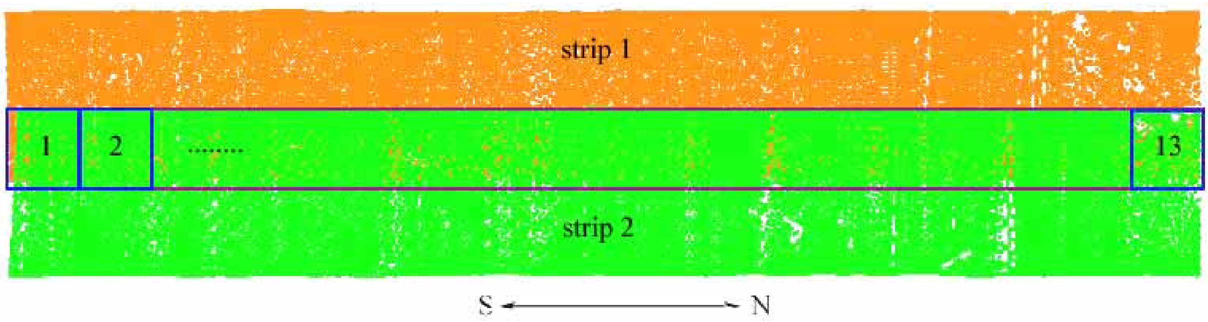

Figure 5.21: Two overlapping laser scanning strips in test site II (*SII*)

The preliminary evaluation by using ground reference points reveals height systematic errors in *SII* (Section 4.5.2). Therefore strip-1 and strip-2 in *SII* are selected to run test flights for this phase of the research. As shown in Figure 5.21, there are thirteen patches selected inside the overlapping area in *SII* as the test patches for the validation with the ICP algorithm.

Table 5.26: Planimetry/height offset, applied to 13 patches of strip-1and 2 for *SII*

Strips	1_2		
No. of patches	13		
Planimetry/Height	X	Y	Z
Average (m)	-0.290	0.280	-0.437
Std dev (m)	0.096	0.072	0.021
Min. (m)	-0.654	-0.031	-0.510
Max. (m)	0.123	0.595	-0.323

The results from applying the ICP algorithm to the planimetry and height offsets in *SII* are presented in Table 5.26 where strip-2 is fixed. The size of the height discrepancy ranges from -0.51 m to -0.32 m while the average height offset is from -0.44 m for all patches. The average planimetric strip shift is -0.29 m in the x direction and 0.60 m in the y direction, accompanying the planimetric shifts up to 0.60 m. With the flight altitude at 1500 m, the horizontal accuracy should be less than 0.75 m. Thus, the detected planimetric shifts between these two neighboring strips are also within the accuracy requirements specified in most ALS systems. However, the identifying height discrepancies suggest that this test set has to be adjusted so as to correct for systematic errors.

The most telling indication of calibration errors can be seen in the graphical profile plot. Like the profiles in *SI*, differences are plainly visible by plotting along structures such as buildings with gable roofs. The significant height discrepancies between two strips can be easily observed from Figure 5.22a. The difference is about 0.43 m and is very close to the result depicted in Table 5.26. The profile generated from the transformed point clouds registered by the ICP algorithm with the strip-2 fixed, shows a much better alignment (Figure 5.22b).

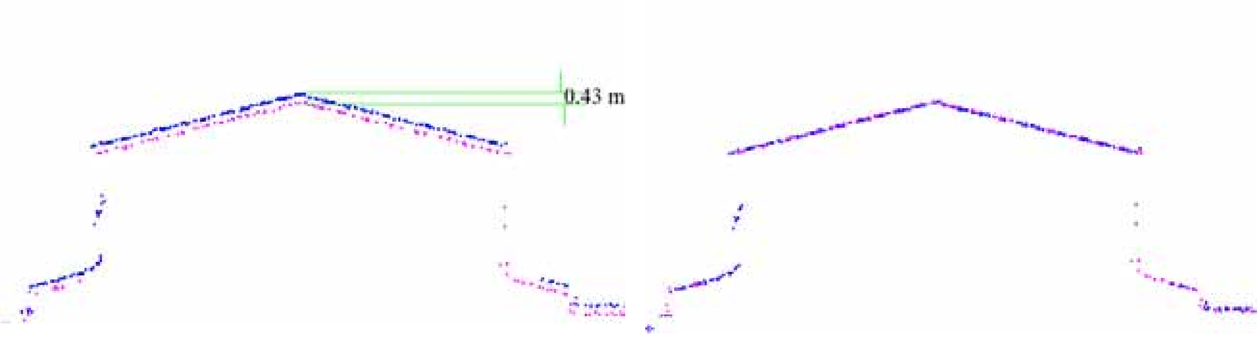

a. Profile from original data b. Profile from data with the ICP matching

Figure 5.22: Profile comparison from 2 overlapping strips for *SII*

Two corresponding, overlapping strips are integrated. As shown in Figure 5.23a, the DSM generated from two original neighboring patches reveals the inconsistency on the surface due to systematic height offsets. Next, the DSM is re-generated by using the registered data to replace the original points for strip 1. Figure 5.23b shows a better agreement on the surface.

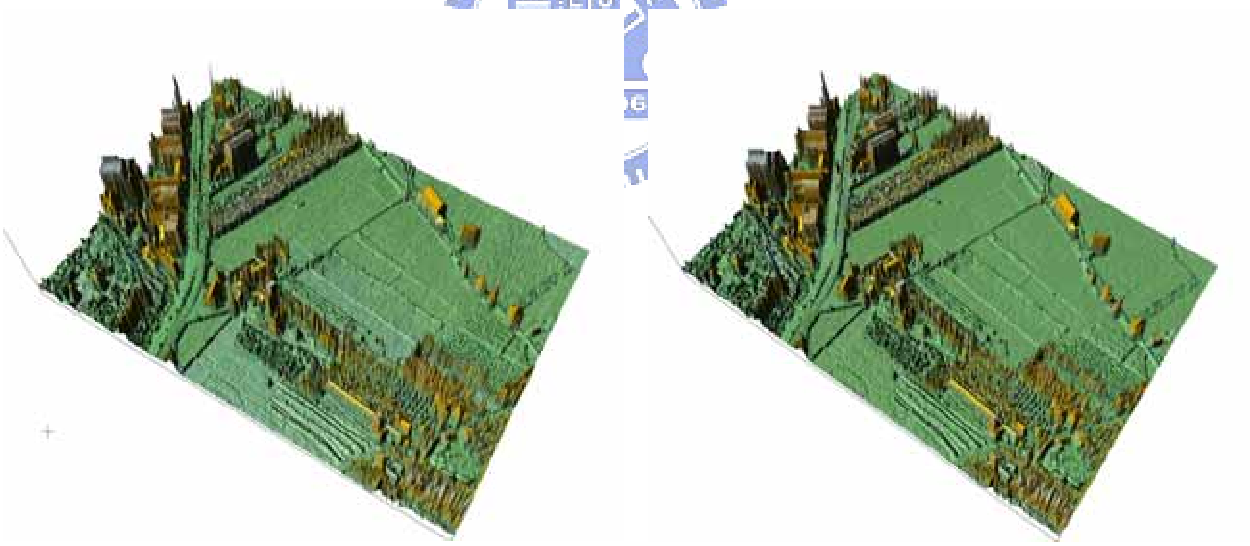

a. From original data. b. From data after the ICP matching when the patch of strip 9 is fixed.

Figure 5.23: DSM of the integrating 2 overlapping strips of patch 1 in *SII*

From the experimental results presented in this section, it can be concluded that the surface registration by using the ICP algorithm can be an alternative way to estimate the height offsets and planimetry shifts from overlapping laser scanning strips. For example, there are not enough ground control points to be used to verify the accuracy of laser data. Moreover, it is not necessary for the ICP algorithm to employ the techniques of interpolation and image processing involved in this step in order to find the corresponding points, which are used as tie points.

5.3 Remaining systematic error recovery

The ICP algorithm plays a successful role not only in estimating the planimetry shifts and height offsets from overlapping laser scanning strips from the analysis of experimental results, but also recovering the imperfect data set based on the assumed perfect data set. However, its convergence onto the desired global minimum requires memory-insensitive and time-consuming implementations. It is not possible to apply the ICP algorithm to two adjacent strips.

Next, this research aims towards presenting a strip adjustment procedure to recover data with remaining systematic errors. Two methods are applied. The 3-D similarity transformation, i.e. the seven parameters transformation between two 3-D data sets, and the strip adjustment with three parameters, are used to adjust the laser strips when there is not enough ground reference points available. Meanwhile, the corresponding points derived from ICP matching are used to form the observations to implement the adjustment.

5.3.1 3-D Similarity Transformation

Test site I (*SI*)

The data validation is followed by data adjustment to fulfill the procedures on handling systematic errors. A 3-D similarity transformation is used to adjust data in this research. In addition to the initial seven parameters, i.e. scale, 3 rotation angles and translation vector, the correspondence between two surfaces have to be established. The correspondence is built when the iteration of surface matching (i.e. the ICP algorithm) terminated.

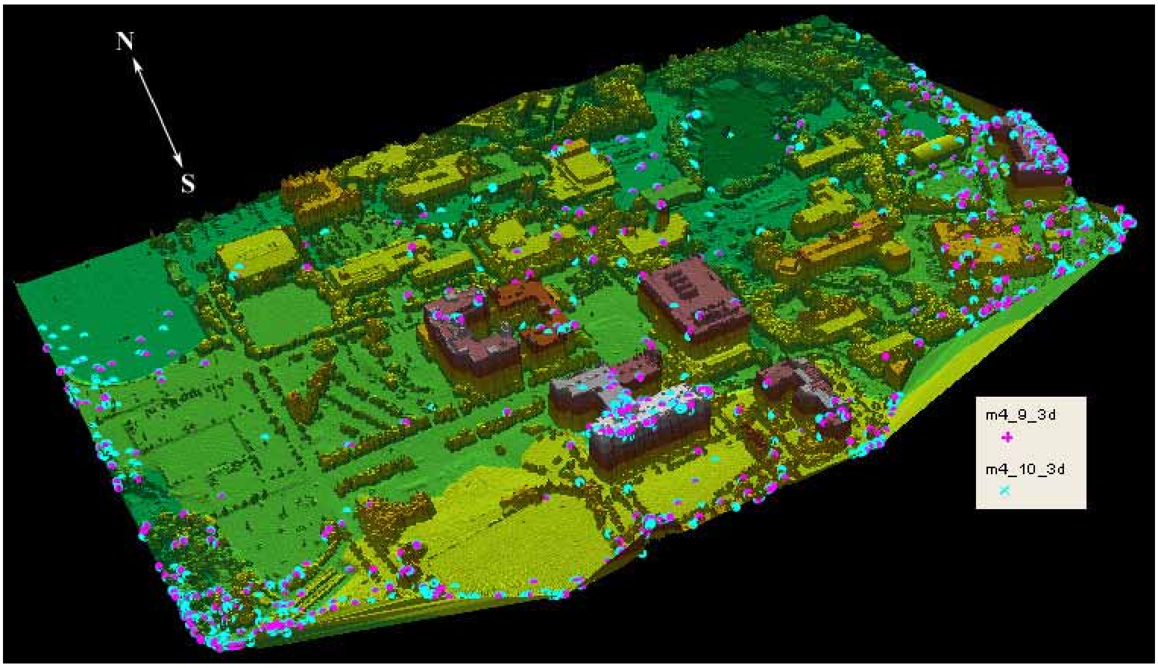

Figure 5.24: Corresponding points for patch 4 of *SI*

The pre-analysis affirms that strip 10 has systematic errors when strip 9 is used as the reference surface. Then strip 9 and strip 10 are chosen as experimental flight lines for *SI*. Again, ICP matching is applied to 14 patches with size of 800 m x 400 m to search the correspondence between strips 9 and 10. The corresponding points, which are derived from all patches, form the input to a 3-D similarity transformation. For example, there are about 900 points that are used to establish the correspondence on patch 4 (NCTU's campus) of *SI*, as shown in Figure 5.24. A generated profile on a roof can tell the position of the corresponding points. The model curve is strip 9 (will be fixed while registering), and the data curve is strip 10 in Figure 5.25a.

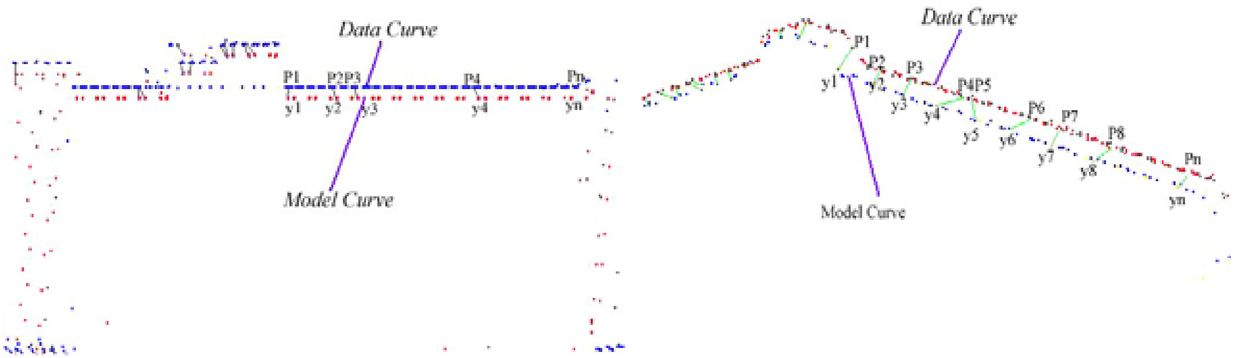

a. Test site I (*SI*)　　　　　　b. Test site II (*SII*)

Figure 5.25: Two examples to show the model curve and data curve

The computed parameters are shown in Table 5.27. It reveals that the systematic error on height is mainly contributed by the misalignment of roll error since the Ω parameter in Table 5.27 is much larger than the accuracy of IMU (0.005 degree for roll & pitch).

Table 5.27: The computed seven parameters for *SI*

Parameters	Scale (λ)	Ω (deg)	Φ (deg)	K (deg)	t_x (m)	t_y (m)	t_z (m)
Value	0.999955	0.018908	-0.000573	0.002865	0.243	-0.387	-1.660

Next, the computed seven parameters are used to recover strip 10. The planimetric and vertical discrepancies are depicted in Table 5.28, and they are computed while calculating the differences of coordinate between the original and the recovered data. The height offset in Table 5.28 is very close to the discrepancies which are derived from surface matching (Section 5.2.1).

Table 5.28: Planimetric/height differences for strip 10 of *SI*

Strips	10		
Planimetry/Height	X	Y	Z
Average (m)	0.267	-0.362	-1.614
Std dev (m)	0.162	0.156	0.079
Min. (m)	-0.055	-0.650	-1.762
Max. (m)	0.552	-0.043	-1.484

In order to find the moving direction and magnitude of strip 10 after transformation, the corresponding points are used as check points. As shown in Figure 5.26, a scaled symbol map using angle values derived from the transformed and original coordinates is superimposed on DSM of patch 4 in strip 10. The scaled arrow in Figure 5.26 is based on the magnitude of the distance between the original and the transformed coordinates. The magnitude ranges from 1.68 m to 1.83 m with an average of 1.73 m and a standard deviation of 0.04 m. The point is generally transformed to its new position along the NW-SE direction.

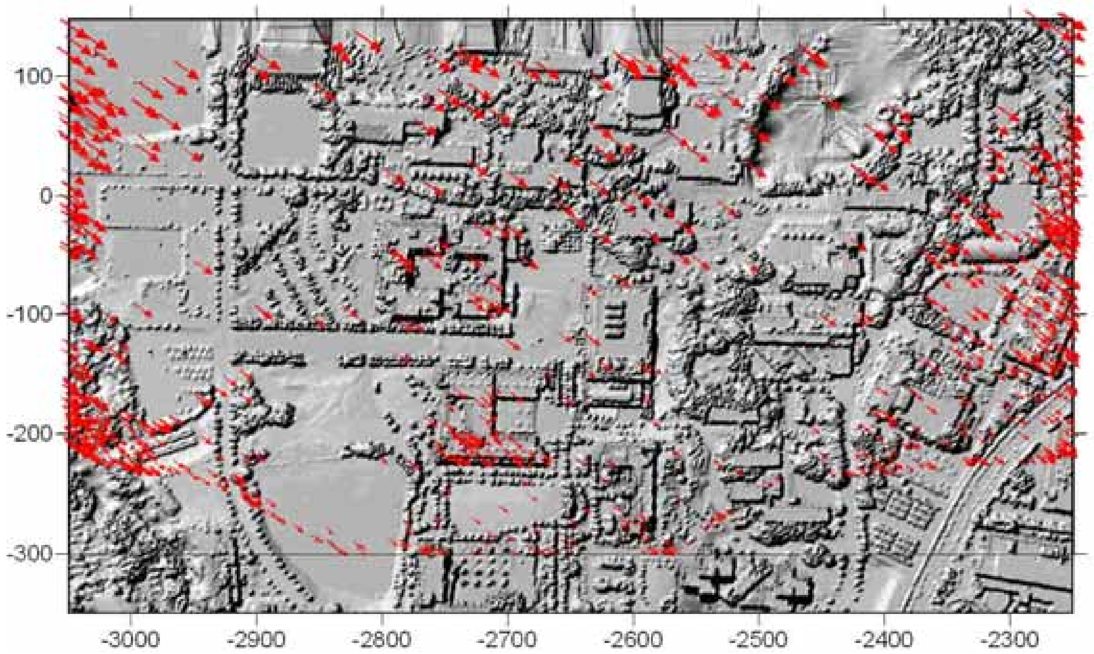

Figure 5.26: A scaled symbol map using angle value (*SI*)

Table 5.29. Height differences before and after data adjustment with GCPs for strip-10

Statistics	Mean(m)	Std dev(m)	Min.(m)	Max.(m)	Qty
Before	1.651	0.102	1.544	1.799	7
After	0.048	0.062	-0.035	0.139	7

Table 5.29 shows that the corresponding points derived from ICP matching that are applied to the 3-D similarity transformation could decrease the average height offsets from 1.65 m to 4.8 cm for strip 10. It suggests that the 3-D similarity transformation provides an alternative way to recover data when there are not enough GCPs.

Test site II (*SII*)

Similarly, the correspondence from thirteen patches of *SII* can be regarded as the tie points when surface matching is done. The 3-D coordinate difference of between the original and the recovered strip 1 is shown in Table 5.31 by using the computed parameters in Table 5.30. Again, the average discrepancy is very close to the result in Section 5.2.2.

Table 5.30: The computed seven parameters for *SII*

Parameters	Scale (λ)	Ω (deg)	Φ (deg)	K (deg)	t_x (m)	t_y (m)	t_z (m)
Value	0.999985	0.000428	-0.00777	0.0004968	-0.299	0.302	-0.468

Table 5.31: Planimetric/height differences for strip 1 of *SII*

Strips	1		
Planimetry/Height	X	Y	Z
Average (m)	-0.279	0.290	-0.437
Std dev (m)	0.020	0.034	0.025
Min. (m)	-0.317	0.230	-0.488
Max. (m)	-0.239	0.352	-0.370

A generated profile on a roof can define the model curve, strip 2 (will be fixed while registering) and the data curve, strip 1 in Figure 5.25b. Next, the corresponding points are used as check points, in order to find the moving direction and magnitude of strip 1 after transformation. As shown in Figure 5.27, a scaled symbol map using angle values derived from the transformed and the original coordinates is superimposed on DSM of patch 2 in strip 1. The magnitude ranges from 0.60 m to 0.63 m with an average of 0.62 m and a standard deviation of 0.8 cm. The point is transformed to its new position along the SE-NW direction.

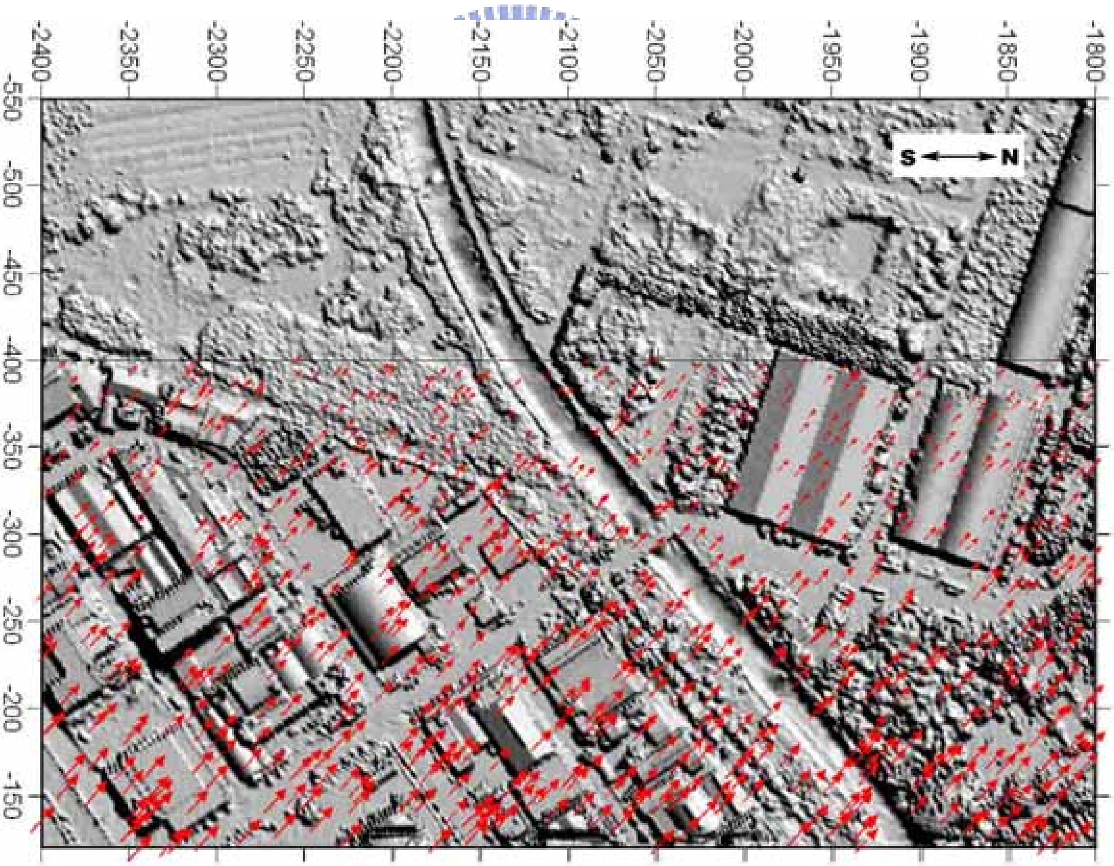

Figure 5.27: A scaled symbol map using angle value (*SII*)

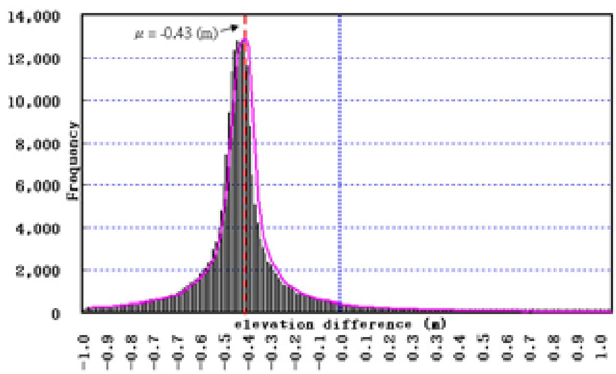

a. Height difference vs. frequency

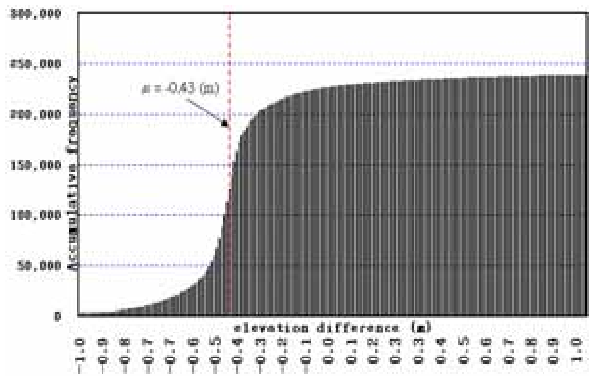

b. Height difference vs. accumulative frequency

Figure 5.28: Height difference between original and transformed patch 2 (*SII*)

Furthermore, the height difference versus frequency, and the height difference versus accumulative frequency are depicted in Figure 5.28a and Figure 5.28b respectively. The average difference (0.43 m) could be considered as the elevation bias between the two strips (strip 1 and strip 2). The probability distribution of the height differences follows approximately a normal distribution.

Correspondingly, Table 5.32 shows that the derived corresponding points could decrease the average height offsets from 0.33 m to -0.10 m for strip 1. For test II, the coordinate of strip 1 is transformed to strip 2 based on the 3-D similarity transformation. The height discrepancy for strip 2, checked by GCPs, reached -0.13 m (Appendix C, Table C.2); thus it results in higher average offsets.

Table 5.32. Height differences before and after data adjustment with GCPs for strip 1

Statistics	Mean(m)	Std dev(m)	Min.(m)	Max.(m)	Qty
Before	0.330	0.026	0.272	0.356	9
After	-0.098	0.045	-0.178	-0.039	9

5.3.2 Strip Adjustment with Three-Parameters

In order to verify the corresponding points from ICP matching, a strip adjustment procedure concerning the heights is used in this section. The method proposed by Crombaghs et al. (2000) and used by Tung (2005) will also apply to two selected test sites.

The foundation of this method is the creation of height differences in overlapping strips. The differences are not computed for individual points because the point noise of about 10-15 cm is high. Therefore, differences are computed as mean differences for groups of minimal 100 points in areas of 50×50 m^2. The "tie points" areas of 50×50 m^2 have to be flat and smooth. Otherwise, small planimetric errors might generate a larger impact on the mean difference for this selected area (Crombaghs et al., 2000). The corresponding points from ICP matching form the "tie points" in this research, instead.

Height differences in overlapping areas of neighboring strips and height differences of laser points and references measurements are used to determine and to correct for offsets and tilts. Every individual strip is corrected for offset (*a*), along-track (*b*), and across-track (*c*) tilts. This method is therefore called the strip adjustment with three parameters.

The reference data (ground control points) are also selected from point clouds since there is not enough ground reference points available. Therefore, the height differences between ground reference points and their corresponding laser points are not presented. The before- and after- adjustment mean height difference and its *RMSE* from corresponding points will be used to evaluate the effect of applying the strip adjustment with three parameters to overlapping strips. The three computed parameters are presented in Table 5.33 for *SI* and *SII*.

Table 5.33: The computed three parameters for *SI* and *SII*

Test Site		offset (*a*)	along-track (*b*)	across-track (*c*)
SI	strip 9	-0.001422	-0.000011	0.000600
	strip 10	-1.594761	-0.000003	0.000111
SII	strip 1	-0.442943	-0.000289	-0.000003
	strip 2	-0.000349	-0.000297	0.000001

The inspection of the adjusting results is done in various ways. One of them is analyzing the spatial distribution of the height residuals after adjustment. Two examples are shown in Figures 5.26 and 5.27 in the previous section. These areas are grouped in pairs, so that the profile of height differences in the along-track direction can be created. Analyzing these profiles of height differences before and after adjustment facilitates the interpretation of the achieved improvement and occurring systematic errors (Crombaghs et al, 2000; Tung, 2005).

Table 5.34: The mean height difference and RMSE for *SI* and *SII*

Test Site	Before adjustment		After adjustment		No. of tie points
	Mean (m)	*RMSE*(m)	Mean (m)	*RMSE*(m)	
SI	-1.619	1.651	0.037	0.294	1184
SII	-0.455	0.487	-0.006	0.173	1843

The mean height differences of corresponding points before adjustment are -1.619 m and -0.455 m for *SI* and *SII*, respectively. These two values are close to the computed parameters of height offset (*a*) which is shown in Table 5.34. It is revealed that the height offset (*a*) is the most significant parameter of systematic errors on height for *SI* and *SII*. Next, the *RMSE* of the residuals after adjustment decreases to 0.294 m from 1.651 m for *SI* and to 0.173 m from 0.487 m for *SII*, respectively.

The effectiveness of the strip adjustment can also be examined by analyzing the distribution of residuals before and after adjustment for whole laser strips. In Figures 5.29 and 5.30, two examples are given. The figure relates to a large block of strips for *SI* and *SII*, respectively. The coordinates of x-axis in Figures 5.29 and 5.30 are the direction of flight, that is, the along-track direction. The residuals are significantly smaller after strip adjustment, leading to the conclusion that the strip adjustment with three parameters increased the quality of dataset considerably.

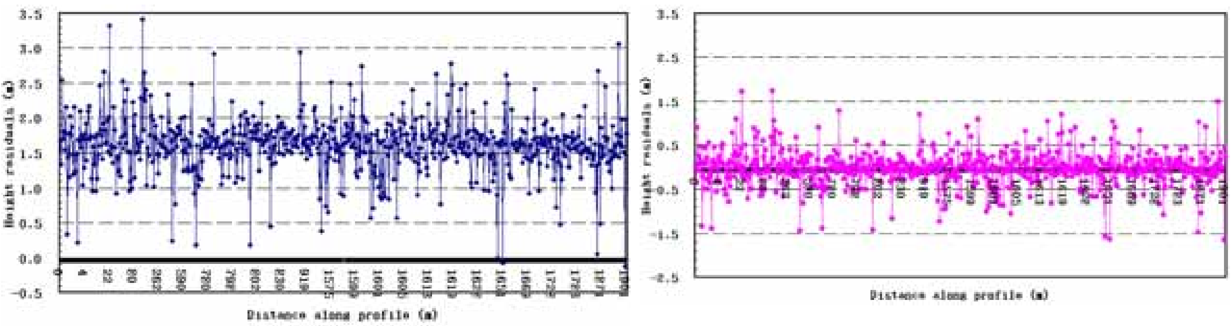

a. Before adjustment b. After adjustment

Figure 5.29: Residuals before and after strip adjustment for *SI*

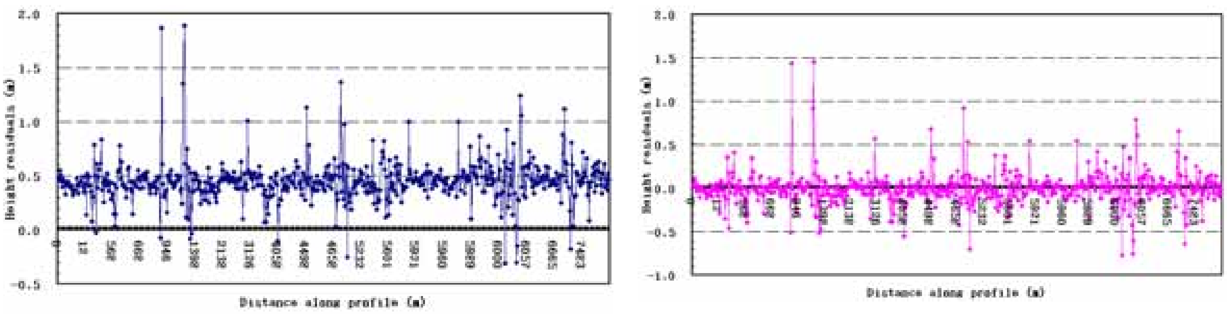

a. Before adjustment b. After adjustment

Figure 5.30: Residuals before and after strip adjustment for *SII*

The decrease of *RMSE* is mainly caused by removing systematic strip errors, such as offset (*a*) and tilts (*b*, *c*). Judged from the results from both test sites, a more sophisticated approach is required. This applies to the deformations, such as cross strip parabolic deformation, along-track periodic effects and strip torsions (Crombaghs et al., 2000).

Applying a 3-D similarity transformation and the strip adjustment with three parameters to a laser scanning data with correspondence derived from surface matching determines the strip discrepancies. It also demonstrates that the accuracy of height can be upgraded if a proper procedure is applied. Nevertheless, the experimental results present a relative accuracy since there is not enough ground reference involved. Therefore, the scheme based on surface matching technique as well as the remaining systematic error recovery can be used as a quality control tool of ALS.

For some digital elevation data, the relative (i.e. point-to-point) accuracy is more important than the absolute accuracy. For example, the relative vertical accuracy of a dataset is especially important for derivative products that make use of the local differences among adjacent elevation values, such as slope and aspect calculations.

Correspondences between overlapping strips of airborne LiDAR serve as the input for strip adjustment procedures that estimate and eliminate systematic errors. In this dissertation, two methodologies are used to establish the correspondence between patches of laser points. First, image matching is used to find the corresponding points (tie points) for boresight calibration. Next, the ICP registration is used for accuracy verification and built the correspondences between overlapping strips. The established correspondences are then used as input data for strip adjustment. Can the matched tie points from overlapping strips via image matching techniques be used as corresponding points for strip adjustment? Or, is it possible that the correspondences from ICP registration can be used as tie points for boresight calibration? The cross-experiments on these issues are presented in Appendix D.

From Appendix D, it can be concluded that the interpolation of laser points to a regular grid introduced errors on the parameters of the 3-D similarity transformation. In addition, it revealed that the interpolation should be avoided while verifying the accuracy of the laser point clouds. Next, with the intentional boresight angles given for calibration, the tie point differences and regular point elevation differences are affected by the large planimetric shifts between the uncalibrated strips. Thus, a grid point in one strip will generally not correspond to the same point in the second strip. To improve the tie point selections by using ICP registration for boresight calibration, it is necessary to address the disadvantages of ICP algorithm.

Finally, the research presented an intensive work on systematic errors for system calibration, systematic error validation and remaining systematic error recovery. The proposed scheme (Figure 5.31) successfully plays a role on data correction as well as on the quality control mechanism for ALS data.

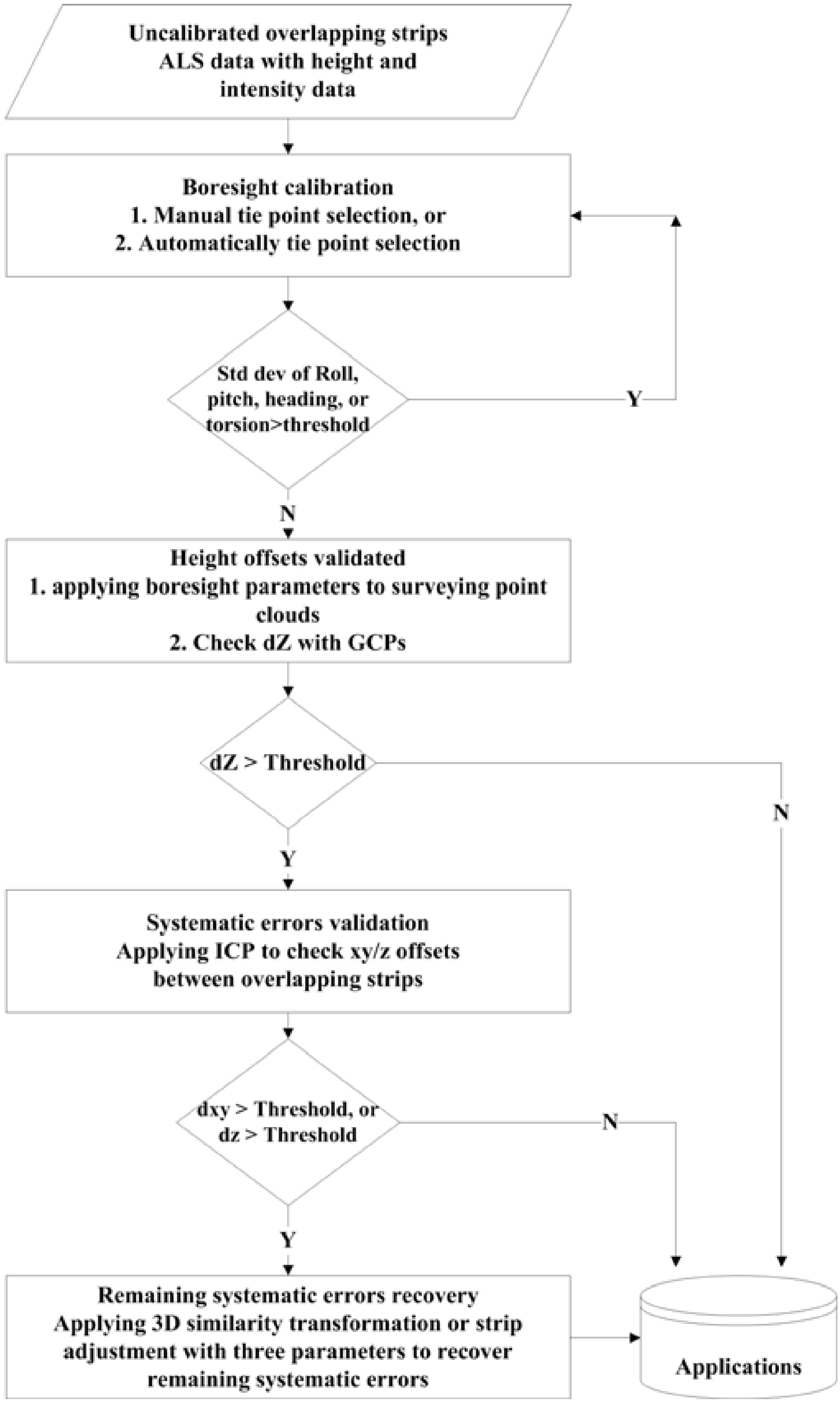

Figure 5.31: Work flows for accuracy assessment on ALS data

CHAPTER 6

CONCLUSION AND FUTURE WORK

This dissertation presents a complete framework on handling systematic errors of ALS data for system calibration, systematic error validation and remaining systematic error recovery. First, for system calibration, each boresight misalignment parameter is discussed to assess its impact on data accuracy and methodology of recovery. A calibration solution used by a commercial system is introduced with a design of optimal calibration flights. The improvement to this approach is then proposed. An in-situ data set from a calibration flight is used to evaluate the improvement on the accuracy of misalignment parameters.

The proposed automated method of extracting tie points to improve the current method on ALS system calibration can significantly upgrade the accuracy in tie point selection. The *TerraMatch* program is then used to re-verify the computed boresight parameters. Therefore, the accuracy of misalignment parameters is expected while applying a practical calibration flight. There is still no standardized procedure on an important issue: how often should the boresight misalignment calibration be checked for an ALS system? With a fast and reliable calibration method, calibration parameters can be checked more frequently. Furthermore, by interpolating intensity reflectance into a regular grid, a grayscale image very similar to photogrammetric images is formed. The similarity was exploited by using an image matching technique to search for the corresponding points. Thus, the intensity information was shown to have high potential for further research.

Next, the ICP algorithm, which is one of the surface registration methods, is adopted in this study to verify the quality of the overlapping laser scanning data. The ICP algorithm provides the benefit of avoiding interpolating raw laser points, and evaluating the height as well as the planimetry offsets from overlapping laser strips. The observed systematic errors in these two data sets also reveal that the accuracy of boresight misalignment parameters plays a critical factor on the quality of point clouds. The correspondence is established, and it is predictable in solving the correspondence problem between two overlapping laser strips.

Next, a strip adjustment procedure is proposed to recover data that have remaining systematic errors. Two methods are applied. The 3-D similarity transformation and the strip adjustment with three parameters are used to recover the laser strips when not enough ground reference points are available. Meanwhile, the corresponding points derived from ICP matching are used to form the observations to implement the adjustment.

The two proposed methods of strip adjustment not only confirm that the corresponding points from ICP matching are good enough observations, but also demonstrate that the two easily implemented methods can improve the quality of ALS data, especially on vertical accuracy. A suggested scheme on the accuracy assessment as well as the strip adjustment for ALS data is therefore proposed.

Furthermore, there are some minor findings from this research. First, the interpolation with a smaller grid size has a higher accuracy of boresight parameters, when the tie points are manually measured with the *Attune* program. However, the laser points are not evenly distributed. The constructed image can sometimes introduce the difficulty for tie point selection when a grid size smaller than the average density of laser points is applied. It is concluded that an interpolation method based on a TIN of the original points with a grid size that relates as closely as possible to the point density at acquisition yields the best results.

The findings based on the correlation matrix of boresight calibration also reveal that the correlations between torsion/roll and torsion/pitch that are generated with an automated tie point selection are much larger than the correlations generated with a manual selection. It implies that the distribution of tie points is correlated with the misalignment parameter's solution.

In this dissertation, the corresponding points that are extracted from the surface registration between two overlapping strips were used as the tie points for data adjustment with the 3-D similarity transformation and the strip adjustment with three-parameters. Before this research goes further to apply more sophisticated approaches to rectify systematic errors, the extracted corresponding points need to be filtered, since some of the pairs are incorrectly matched. The examples include points on moving vehicles, points on trees, or points falling into occluded zones. The appropriate solution could (i) apply image matching to filter out points locating on a distinctive feature such as road marking or intersections, and (ii) use the classified ground laser points for ICP matching to avoid selecting points on vegetation or inside of occluded zones.

The present work recommends future research with respective to the following topics:

- Traditionally, the accuracy of manual tie point measurement should reach *ps*/3 (*ps* = pixel size) in digital photogrammetry. The intensity images used in the *Attune* program and the height/intensity images used in this dissertation are based on interpolated regular grid. Therefore, these images are much different from traditional photogrammetric images. Furthermore, the size of laser footprint varies with the strength of reflectance and the factors of terrain. In practical test, this level (*ps*/3) of accuracy is very difficult to reach while applying manual tie point selection. With the innate limitation of horizontal accuracy of ALS data, how to set up the standard of accuracy on the tie point measurement for ALS interpolated data will be an issue that requires further research.

- Regarding the distribution of points, it is difficult to force the computer to 'find' a solution in a desired zone while implementing image matching to find the corresponding points. On the contrary, an operator can easily select the points with a priori knowledge on geometric distribution. Xu (2004) proposed a mechanism to split the matching areas into nine (or more) rectangles to make sure that each rectangle has at least one successfully-matched point. Considering the characteristics of induced errors, the solution of boresight misalignment parameters might be sensitive to the geometry of the selected tie points. It suggests that geometric distribution of corresponding points on the effects upon solution of parameters is one of the critical issues for future investigation.

- For the ICP algorithm as well as other registration methodologies, refinement of the algorithm is necessary. Firstly, a more functional algorithm to remove the effects that are introduced by occlusions should be applied before matching. Next, as a consequence of the characteristics of laser pulse penetration as well as sampling pattern and viewing direction, data points on vegetation or other objects with an irregular shape may show rather different heights in neighbouring strips, leading to unpredictable outliers in matching. It suggests that the classified ground points should be applied for matching.

- Including the proposed surface matching algorithm in this study, some of the strip adjustment methods work only with tie points without using GCPs. However, the use of some type of ground control is desirable, since eliminating the relative discrepancies between overlapping strips does not provide an absolute check of the data sets. An efficient and realizable method to find the correspondence between laser points and ground is essential. Specifically-designed ALS targets similar to Csanyi et al. (2005) should be considered for future research on ALS strip adjustment.

BIBLIOGRAPHY

Ackermann, F., 1999. Airborne Laser Scanning－Present Status and Future Expectations. *ISPRS Journal of Photogrammetry and Remote Sensing,* 54 (2-3), pp. 64-67.

Ahokas, E., H. Kaartinen, and J. Hyyppa, 2004. A Quality Assessment of Repeated Airborne Laser Scanner Observations. *Proceedings of the XXth ISPRS Congress*, Istanbul, Turkey, Jul. 12-23.

Alharthy, A., J. Bethel, E. M. Mikhail, 2004. Analysis and Accuracy Assessment of Airborne Laser Scanning System. *Proceedings of the XXth ISPRS Congress*, Istanbul, Turkey, Jul. 12-23.

Applanix, 2004. System Specifications － POS AV DG Model 501 (URL:http://www.applanix.com/products/posav_index.php).

Artuso, R., S. Bovet, and A. Streilein, 2003. Practical Methods for the Verification of Countrywide Terrain and Surface Models. *ISPRS Workshop on 3-D Reconstruction from Airborne Laserscanner and InSAR Data*, Dresden, Germany, Oct. 8-10

ASPRS, 2000. Vegetation Identification and Classification Using Lidar Data. *ASPRS-ACSM Workshop on Practical Applications in the Geospatial Information Sciences*, Rhode Island, Dec. 1-6.

Axelsson, P., 1999. Processing of Laser Scanner Data－Algorithms and Applications. *ISPRS Journal of Photogrammetry and Remote Sensing,* 54 (2-3), pp. 138-147.

Baltsavias, E. P., 1999a. A comparison Between Photogrammetry and Laser Scanning. *ISPRS Journal of Photogrammetry and Remote Sensing,* 54 (2-3), pp. 83-94.

Baltsavias, E. P., 1999b. Airborne Laser Scanning: Existing Systems and Firms and Other Resources. *ISPRS Journal of Photogrammetry and Remote Sensing,* 54 (2-3), pp. 164-198.

Baltsavias, E. P., 1999c. Airborne Laser Scanning: Basic Relations and Formula. *ISPRS Journal of Photogrammetry and Remote Sensing,* 54 (2-3), pp. 199-214.

Behan, A., 2000. On the Matching Accuracy of Rasterized Scanning Laser Altimeter Data. *International Archives of Photogrammetry and Remote Sensing*, vol. 33, part B2, pp. 75-82.

Behan, A., H.-G. Maas, and G. Vosselman, 2000. Steps towards Quality Improvement of Airborne Laser Scanner Data. *Proceedings of the 26th Annual Conference of the Remote Sensing Society* (URL:http://www.geo.tudelft.nl/frs/papers/2000/behan2000_quality.pdf).

Berg, R. and J. Ferguson, 2001. Airborne Laser Mapping for Highway Engineering Applications. *Proceedings of the ASPRS Annual Conference*, St. Louis, USA.

Besl, P. and N. McKay, 1992. A Method of Registration of 3-D Shapes, *IEEE Trans. PAMI 12*.

Blair, B., D. L. Rabine and M. Hofton, 1999. The Laser Vegetation Image Sensor: A Medium-altitude, Digitization-only, Airborne Laser Altimeter for Mapping Vegetation and Topography. *ISPRS Journal of Photogrammetry and Remote Sensing,* 54 (2-3), pp. 115-122.

Briese, C. and N. Pfeifer, 2001. Airborne Laser Scanning and Derivation of Digital Terrain Models. *Proceedings of the Optical 3D Measurement Techniques*, Vienna, Austria, Oct. 1-4, pp. 80-87.

Brugelmann, R. Automatic Breakline Detection from Airborne Laser Range Data. *Proceedings of International Archives of Photogrammetry and Remote Sensing*, Vol. XXXIII, Part B3, Amsterdam.

Burman, H., 2000a. Adjustment of Laserscanner Data for Correction of Orientation Errors. *International Archives of Photogrammetry and Remote Sensing*, vol. 33, part B3/1, pp. 125-132.

Burman, H., 2002b. Calibration and Orientation of Airborne Image and Laser Scanner Data Using GPS and INS. Ph. D. Dissertation, Royal Institute of Technology, 111 pages.

Burman, H., 2002. Laser Strip Adjustment for Data Calibration and Verification. In *ISPRS Commission III, Symposium 2002, Graz, Austria*, pp. 067-072.

Burman, H. and A. Soininen, 2004. *TerraMatch User's Guide*. TerraSolid Inc., 44 pages.

Carter, W., R. Shrestha, G. Tuell, M. Sartori and D. Bloomquist, 2001. Airborne Laser Swath Mapping. University of Florida (URL: http://www.alsm.ufl.edu/).

Casella, V., 2003. Accuracy Assessment of Laser Scanning Data, Department of Building and Territorial Engineering. University of Pavia, Italy (URL:http://www.inf.uni-konstanz.de/cgip/lehre/ss03-proj/papers/Casella01.pdf).

Chen, W. Y., 2000. A Study on the Wavelet Theory Applied to Image Registration. Master Thesis, Department of Civil Engineering, National Chiao Tung University, Hsinchu, Taiwan, 66 pages.

Chen, Y. and G. Mediono, 1991. Object Modeling by Registration of Multiple Range Views. *Proceedings of International Conference on Robotics and Automation.*

Chui, H. and A. Rangarajan, 2003. A New Point Matching Algorithm for Non-rigid Registration. *Computer Vision and Image Understanding*, Vol. 89, pp. 114-141.

CHSurvey Co. LTD., 2005. *Optech ALTM7030 Calibration Report*, 18 pages (in Chinese).

Crombaghs, M., R. Brügelmann, and E. de Min, 2000. On the Adjustment of Overlapping Strips of Laseraltimetrt Heigh Data. *International Archives of Photogrammetry and Remote Sensing*, vol. 33, part 3A, pp. 230-237.

Csanyi, N. and C. K. Toth, 2004. On using Lidar Specific Ground Targets. *Proceedings of the ASPRS Annual Conference*, Denver, May. 23-28.

Csanyi, N., C. K. Toth, D. Grejner-Brzezinska, and J. Ray, 2005. Improvement of Lidar Data Accuracy Using Lidar Specific Ground Targets. *ASPRS Annual Conference*, Baltimore, Mar. 7-11.

Dijkman, S. T. and F. A. Heuvel, 2002. Semi Automatic Registration of Laser Scanner Data. *International Archives of Photogrammetry and Remote Sensing*, Vol. 34, Part 5, Corfu, Greece, Sep. 2-6, pp. 12 – 17.

Dufournaud, Y., C. Schmid and R. Horaud, 2004. *Image Matching with Scale Adjustment. Computer Vision and Image Understanding*, Vol. 93, pp. 175-194.

Elberink, S. O., G. Brand, and R. Brugelmann, 2003. Quality Improvement of Laser Altimetry DEM'S. *ISPRS Workshop on 3-D Reconstruction from Airborne Laserscanner and InSAR Data*, Dresden, Germany, Oct. 8-10.

Filin, S., 2001. Calibration of Airborne and Spaceborne Laser Altimeters Using Nature Surfaces. Ph. D. Dissertation, Graduate School of The Ohio State University, 128 pages.

Filin, S., B. Csathó, and T. Schenk, 2001. An Analytical Models for In-fight Calibration of Laser Altimeter Systems Using Natural Surfaces. *Proceedings of the ASPRS Annual Conference*, St. Louis, USA.

Filin, S., 2003. Recovery of Systematic Biases in Laser Altimetry Data Using Natural Surfaces. *Photogrammetric Engineering and Remote Sensing*, Vol. 69, No. 11, pp. 1235-1242.

Flood, M., 2001. LIDAR Activities and Research Priorities in the Commercial Sector. *International Archives of Photogrammetry and Remote Sensing*, WG IV/3, Vol. XXXIV, Annapolis, MD, Oct. 22-24, pp. 678-684.

Forstner, W., 1986. A Feature Based Correspondence Algorithm for Image Matching. *Proceedings of International Archives of Photogrammetry and Remote Sensing*, 26(B3/3), pp. 13-19.

Forstner, W. and E. Gulch, 1987. A Fast Operator for Detection and Precise Location of Distinct Point, Corners and Center of Circular Features. *Proceedings of the Intercommision of the ISPRS*, Interlaken, Switzerland, pp. 281-305.

Forsyth, D. A. and J. Ponce, 2003. *Computer Vision A Modern Approach*. Prentice Hall, 693 pages.

Golden Software, 1997. Surfer User's Guide Version 6: Contouring and 3D Surface Mapping. Golden Software, Inc., 24 chapters.

Gutierrez, R. J. C. Gibeaut, R. C. Smyth, T. L. Hepner, J. R. Andrews, C. Weed, W. Gutelius and M. Mastin, 2001. Precise Airborne Lidar Surveying for Coastal Research and Geohazards Applications. *International Archives of Photogrammetry and Remote Sensing*, Vol. XXXIV-3/W4, Annapolis, MD, Oct. 22-24.

Haala, N. and C. Brenner, 1999. Extraction of Buildings and Trees in Urban Environments. *ISPRS Journal of Photogrammetry & Remote Sensing*, 54(2-3), pp. 130-137.

Hajnal, J. V., D. L. Hill, and D. J. Hawkes, 2001. *Medical Image Registration*. CRC Press, 382 pages.

Harding, D. J., M.A. Lefsky, G.G. Parker, and J.B. Blair, 2001. Laser Altimeter Canopy Height Profiles: Methods and Validation for Closed-canopy, Broadleaf Forests. *Remote Sensing of Environment*, Vol.76, pp. 283-297.

Harris, C. and M. Stephens, 1988. A Combined Corner and Edge Detector. *In Fourth Alvey Vision Conference*, Manchester, pp. 147-151.

Hentschel, M., 2005. Personnel communication.

Hodgson, M. E. and P. Bresnahan, 2004. Accuracy of Airborne Lidar-derived Elevation: Empirical Assessment and Error Budget. *Photogrammetric Engineering and Remote Sensing*, Vol. 70, No. 3, pp. 331-339.

Hofton, M., J. B. Minster and B. Blair, 2000. Decomposition of Laser Altimetry Waveforms. *IEEE Trans. on Geoscience and Remote Sensing*, Vol.38, No. 4, pp. 1989-1996.

Hsieh, J. W., H. Y. Liao, K. C. Fan, M. T. Ko and Y. P. Hung, 1997. Image Registration Using a Edge-Based Approach. *Computer Vision and Image Understanding*, Vol. 67, No. 2, pp. 112-130.

Huising, E. J. and L. M. Gomes Pereira, 1998. Errors and Accuracy Estimates of Laser Data Acquired by Various Laser Scanning Systems for Topographic Applications. *ISPRS Journal of Photogrammetry and Remote Sensing,* 53 (5), pp. 245-261.

Hwang, C., 2001. ICV5641: *Adjustment Theory*. Class Notes, Department of Civil Engineering, National Chiao Tung University.

Irish, J. L. and W. J. Lillycrop, 1999. Scanning Laser Mapping of the Coastal Zone: the SHOALS system. *ISPRS Journal of Photogrammetry & Remote Sensing*, 54(2-3), pp.123-129.

ITRI, 2004. *High Accuracy and High Resolution DTM Mapping and Database Establishment for the Lidar Survey Areas and the Developments of their Application*. Interim Report No.1, Ministry of Interior, Taiwan, 125 pages (in Chinese).

ITRI, 2005. *High Accuracy and High Resolution DTM Mapping and Database Establishment for the Lidar Survey Areas and the Developments of their Application*. Interim Report No.2, Ministry of Interior, Taiwan, 141 pages (in Chinese).

Kager, H. 2004. Discrepancies between Overlapping Laser Scanning Strips-simultaneous Fitting of Aerial Laser Scanner Strips. *Proceedings of the XXth ISPRS Congress*, Istanbul, Turkey, Jul. 12-23.

Kao, Y. H., 2005. Personnel communication.

Kasser, M. and Y. Egels, 2002. *Digital Photogrammetry*. Taylor & Francis, 351 pages.

Katzenbeisser, R., 2003. About the Calibration of Lidar Sensors, *ISPRS Workshop on 3-D Reconstruction from Airborne Laserscanner and InSAR Data*. Dresden, Germany, Oct. 8-10.

Kilian, J., N. Haala, and M. Englich, 1996. Capture and evaluation of airborne laser scanner data. *International Archives of Photogrammetry and Remote Sensing*. Vol. 31, part B3, Vienna, pp. 383-388.

Kornus, W. and A. Ruiz, 2003. Strip Adjustment of LIDAR Data. *ISPRS Workshop on 3-D Reconstruction from Airborne Laserscanner and InSAR Data*. Dresden, Germany, Oct. 8-10.

Krabill, W.B., C.W. Wright, R. N. Swift, E. B. Frederick, S. S. Manizade, J. K. Yugel, C. F. Martin, J. G. Sonntag, M. Duffy, W. Hulslander, and J. C. Brock, 2000. Airborne Laser Mapping of Assateague National Seashore Beach. *Photogrammetric Engineering & Remote Sensing*, Vol. 66, No. 1, pp. 65-71.

Kraus, K. and N. Pfeifer, 1997. A New Method for Surface Reconstruction from Laser Scanner Data. *International Archives of Photogrammetry and Remote Sensing*, Vol. 32, part B3, pp. 80-86.

Kraus, K. and N. Pfeifer, 1998. Determination of Terrain Models in Wooded Areas with Airborne Laser Scanner Data. *ISPRS Journal of Photogrammetry and Remote Sensing,* Vol. 53, pp. 193-203.

Kraus, K. and N. Pfeifer, 2001. Advanced DTM Generation from Lidar Data. *International Archives of Photogrammetry and Remote Sensing*, Vol. XXXIV-3/W4, Annapolis, MD, Oct. 22-24.

Kropatsch, W. G. and H. Bischof, 2001. *Digital Image Analysis – Selected Techniques and Applications*. Springer, 505 pages.

Latypov, D., 2002. Estimating Relative Lidar Accuracy Information from Overlapping Flight Lines. *ISPRS Journal of Photogrammetry and Remote Sensing,* Vol. 56, pp. 236-245.

Lee, I., 2002. Perceptual Organization of Surfaces, Ph. D. Dissertation, Graduate School of The Ohio State University, 159 pages.

Lee, B. K., K. Yu, and M. Pyeon, 2003. Effective Reduction of Horizontal Error in Laser Scanning Information by Strip-wise Least Squares Adjustment. *Electronics and Telecommunications Research Institute Journal* (Korea), Vol. 25, no. 2, pp. 109-120.

Leica, 2002. ALS40 Airborne Laser Scanner, Leica Geosystems GIS & Mapping. LLC (URL:http://gis.leica-geosystems.com /Products/).

Leica, 2003a. *ALS Calibration Attune Operation Manual Revision 2*. Leica Geosystems GIS & Mapping, LLC, 43 pages.

Leica, 2003b. ALS50 Workshop Outline. *Leica Geosystems User Group Meeting and Aerial Sensor Workshop*, Denvor, USA, Aug. 18-21.

Leica, 2004a. Overview on ALS50 Airborne Laser Scanner. Leica Geosystems GIS & Mapping, LLC (URL: http://gis.leica-geosystems.com/products/als50/default.asp).

Leica, 2004b. ALS50 Airborne Laser Scanner User Guide. Leica Geosystems GIS & Mapping, LLC (URL: http://gis.leica-geosystems.com/products/als50/default.asp).

Lin, H. T., 2002. Autonomous Recovery of Exterior Orientation of Imagery Using Free-Form Linear Features. Ph. D. Dissertation, Graduate School of The Ohio State University, 110 pages.

Liu, J. K., W. C. Hsu and T. Y. Shih, 2005. A Study on Investigation and Implement of ALS Boresight Calibration. *Journal of Surveying Engineering*, Vol.47, No.2, pp.49-66 (in Chinese).

Lohmann, P. and A. Koch, 1999. Quality Assessment of Laser-Scanner-Data. *Joint Workshop of ISPRS WG I/1, I/3, and I/4, on Sensor and Mapping from Space*, Hannover, Germany.

Luhmann, T. and G. Altrogge, 1986. Interest-Operator for Image Matching. *Proceedings of International Archives of Photogrammetry and Remote Sensing*, Vol. 26, part-B3, pp. 459-474.

Lutz, E. Th. Geist and J. Stotter, 2003. Investigation of Airborne Laser Scanning Signal Intensity on Glacial Surfaces – Utilizing Comprehensive Laser Geometry Modeling and Orthophoto Surface Modeling. *ISPRS Workshop on 3-D Reconstruction from Airborne Laserscanner and InSAR Data*, Dresden, Germany, Oct. 8-10.

Maas, H-G. and G. Vosselman, 1999. Two Algorithms for Extracting Building Models from Raw Laser Altimetry Data. *ISPRS Journal of Photogrammetry & Remote Sensing*, 54(2-3), pp. 153-163.

Maas, H.-G., 2000. Least Squares Matching with Airborne Laserscanning Data in a TIN Structure. *International Archives of Photogrammetry and Remote Sensing*, Vol. 33, Part 3A, pp. 548-555.

Maas, H.-G., 2001. On the Use of Pulse Reflectance Data for Laserscanner Strip Adjustment. *ISPRS Workshop on Land Surface Mapping and Reconstruction using Laser Altimetry*, Annapolis, MD, IAPRS Vol. XXXIV, Part 3/W4.

Maas, H.-G., 2002. Methods for Measuring Height and Planimetry Discrepancies in Airborne Laserscanner Data. *Photogrammetric Engineering and Remote Sensing*, Vol. 68, No. 9, pp. 933-940.

Maas, H.-G., 2003. Planimetric and Height Accuracy of Airborne Laserscanner Data - User Requirements and System Performance. Proceedings 49, Photogrammetric Week (Ed. D. Fritsch), Wichmann Verlag, pp. 117-125.

Mathworks, 2004. MATLAB Function Reference. The Mathworks Inc., (URL:http://www.mathworks.com/access/helpdesk/help/techdoc/ref/griddata.html).

McIntosh, M., K. Krupnik and A. Schenk, 2000. Improvement of Automatic DSM Generation over Urban Areas Using Airborne Laser Scanner Data. *Proceedings of International Archives of Photogrammetry and Remote Sensing*, Vol. XXXIII, Part B3, Amsterdam.

Merrick, 2003. Statement of Qualification to Provide Lidar Services. Merrick Inc. (URL:http://www.merrick.com/services/gis/LIDAR_SOQ_Internet.pdf).

Mikhail, E. M., J. S. Bethel and J. C. McGlone, 2001. *Introduction to Modern Photogrammetry*. John Wiley & Sons, 479 pages.

Mitchell, H. L., J. G. Fryer, and R. Paquet, 2002. Integration and Filtering of 3D Spatial Data Using a Surface Comparison Approach. *ISPRS Commission IV Symposium 2002*, Ottawa, Canada.

Morin, K. and N. El-sheimy, 2002. Post-mission Adjustment Methods of Airborne Laser Scanning Data. *FIG XXII International Congress*, Washington, D.C. USA.

Morin, K., 2002. Calibration of Airborne Laser Scanners. Master Thesis, Department of Geomatics Engineering, University of Calgary, 125 pages.

Mostafa, M. M. R., 2001. Digital Multi-Sensor Systems-Calibration and Performance Analysis. *OEEPE Workshop*, *Integrated Sensor Orientation*, Hannover, Germany, Sep. 17-18.

Murakami, H., K. Nakagawa, H. Hasegawa, T. Shibata, and E. Iwanami, 1999. Change Detection of Buildings Using an Airborne Laser Scanner. *ISPRS Journal of Photogrammetry & Remote Sensing*, 54(2-3), pp. 148-152.

Nikolaidis, N. and I. Pitas, 2001. *3-D Image Processing Algorithms*. John Wiley & Sons, 176 pages.

Optech, 2002. ALTM Airborne Laser Terrain Mappers. Optech Inc. (URL:http://www.optech.on.ca/).

Optech, 2003. Processing Calibration Steps. Optech Inc., 7 pages.

Optech, 2004. ALTM Applications. Optech Inc. (URL:http://www.optech.ca/altmapps.htm).

Paquet, R., 2003. A Method to Predict Accuracy of Least Squares Surface Matching for Airborne Laser Scanning Data Sets. *ISPRS Workshop on 3-D Reconstruction from Airborne Laserscanner and InSAR Data*, Dresden, Germany, Oct. 8-10.

Riano, D., E. Meier, B. Allgöwer, E. Chuvieco and S. L. Ustin, 2003. Modeling Airborne Laser Scanning Data for the Spatial Generation of Critical Forest Parameters in Fire Behavior Modeling. *Remote Sensing Environment*, 86(2), pp.177-186.

Ronnholm, P. 2004. The Evaluation of the Internal Quality of Laser Scanning Strips Using the Interactive Orientation Method and Point Clouds. *Proceedings of the XXth ISPRS Congress*, Istanbul, Turkey, Jul. 12-23.

Schenk, T., 1999. *Digital Photogrammetry Volume I - Background, Fundamentals, Automatic Orientation Procedures*. TerraScience, 428pages.

Schenk, T., 2001. Modeling and Analyzing Systematic Errors of Airborne Laser Scanners. Technical Notes in Photogrammetry No. 19. Department of Civil and Environmental Engineering and Geodetic Science, The Ohio State University, Columbus, Ohio, 40 pages.

Schenk, T. S. Suyoung, and B. Csatho, 2001. Accuracy Study of Airborne Laser Scanning Data with Photogrammetry. *International Archives of Photogrammetry and Remote Sensing*, WG IV/3, Vol. XXXIV, Annapolis, MD, Oct. 22-24, pp.113-118.

Schmid, C., R. Mohr, and C. Bauckhage, 2000. Evaluation of Interest Point Detectors. *International Journal of Computer Vision*, Vol. 37, No. 2, pp. 151-172.

Shih, T. Y. and M. H. Peng, 2003. An Evaluation of Lidar and Photogrammetrically-collected DEMs. Council of Agriculture, Taiwan (In Chinese).

Sithole, G. and G. Vosselman, 2003. Comparison of Filtering Algorithms. *ISPRS Workshop on 3-D Reconstruction from Airborne Laserscanner and InSAR Data*, Dresden, Germany, Oct. 8-10.

Soininen, A., 2004. *TerraScan User's Guide*. TerraSolid Inc., 158 pages.

Song, J., S. Han, K. Yu, and Y. Kim, 2002. Assessing the Possibility of Land-cover Classification Using Lidar Intensity Data. *ISPRS Photogrammetric Computer Vision Symposium*, Graz, Austria.

Sun, G. and J. K. Ranson, 2000. Modeling Lidar Return from Forest Canopy. *IEEE Trans. on Geoscience and Remote Sensing*, Vol.38, No. 6, pp. 2617-2626.

Terrasolid, 2004. Terrasolid Applications for Geo-Engineering. Terrasolid Inc. (URL:http://www.terrasolid.fi/).

TopEye AB, 2006. Introduction to TopEye MK II (URL:http://www.topeye.com/system.htm).

Tung, J. S., 2005. Airborne Lidar Systematic Error Analysis and Strip Adjustment. Master Thesis, Department of Geomatics, National Cheng Kung University, 83 pages.

Vaughn, C. R., J. L. Bufton, W. B. Krabill and D. Rabine, 1996. Georeferecing of Airborne Laser Altimter Measurements. *International Journal of Remote Sensing*, Vol. 17, No. 11, pp. 2185-2200.

Vosselman, G., and H.-G. Maas, 2001. Adjustment and Filtering of Raw Laser Altimetry Data. *OEEPE Workshop on Airborne Laserscanning and Interferometric SAR for Detailed Digital Elevation Models*, Stockholm, Mar. 1-3.

Vosselman, G., 2002a. On the Estimation of Planimetric offsets in Laser Altimetry Data. *International archives of Photogrammetry and Remote Sensing*, Vol. 34, Part 3A + B, Graz, Sep. 9-13, pp. 375 -380.

Vosselman, G., 2002b. Strip Offset Estimation Using Linear Features. *The 3rd International Workshop on Mapping Geo-Surfical Processes Using Laser Altimetry Columbus*, Ohio, USA, Oct. 7-9.

Watson, D., 1992. *Contouring: A Guide to the Analysis and Display of Spatial Data*. Pergamon Inc., 321 pages.

Wehr A., Lohr U., 1999. Airborne Laser Scanning – an Introduction and Overview. *ISPRS Journal of Photogrammetry and Remote Sensing*, 54 (2-3), pp. 68-82.

Xu, F., 2004. Mapping and Localization for Extraterrestrial Robotic Explorations. Ph. D. Dissertation, Graduate School of The Ohio State University, 158 pages.

Zhang, Z, 1994. Iterative Point Matching for Registration of Free-Form Curves and Surfaces. *International Journal of Computer Vision*, 1994.

Ziegler, M., A. Wimmer and R. Wack, 2001. DTM Generation by Means of Airborne Laser Scanning – An Advanced Method for Forest Areas. *Proceedings of the Optical 3D Measurement Techniques*, Vienna, Austria, Oct. 1-4, pp. 97-102.

Appendix A: Observation equation of proposed methodology for ALS boresight calibration

For each ground or tie point from an ALS data can be described as a parametric equation as:

$$\begin{bmatrix} X \\ Y \\ Z \end{bmatrix}_{\substack{ground \\ control}} = \begin{bmatrix} X \\ Y \\ Z \end{bmatrix}_{\substack{aircraft \\ position}} + R_{\substack{body \\ frame \\ to \\ ground \\ rotation}} \cdot R_{misalignment} \begin{bmatrix} l_x \\ l_y \\ l_z \end{bmatrix}_{\substack{laser \\ range \\ components}} \tag{A-1}$$

where:

$(X,Y,Z)_{groundcontrol}$: the derived terrain point

$(X,Y,Z)_{aircraftposition}$: the aircraft position at the observation epoch

$R_{body\ to\ ground\ rotation}$: the rotation cosine matrix from the aircraft body frame to the ground frame

$(l_x, l_y, l_z)_{laserrange}$: the laser range components derived from the laser range and scanner angle

It has been observed empirically that the misalignment angles are often less than 3 degrees. The misalignment matrix $R_{misalignment}$ is therefore replaced by the small-angle approximation:

$$R_{misalignment} = \begin{bmatrix} 1 & -\kappa & \phi \\ \kappa & 1 & -\omega \\ -\phi & \omega & 1 \end{bmatrix} \tag{A-2}$$

where:

ω, ϕ, κ : the roll, pitch, and heading misalignment angles

From Equations (A-1) and (A-2), it can be derived:

$$\begin{bmatrix} X_1 \\ Y_1 \\ Z_1 \end{bmatrix} = \begin{bmatrix} 1 & -\kappa & \phi \\ \kappa & 1 & -\omega \\ -\phi & \omega & 1 \end{bmatrix} \cdot \begin{bmatrix} l_X \\ l_Y \\ l_Z \end{bmatrix}_{\substack{laser \\ range \\ components}} \tag{A-3}$$

where:

$$\begin{bmatrix} X_1 \\ Y_1 \\ Z_1 \end{bmatrix} = R^T_{\substack{body\\frame\\to\\ground\\rotation}} \left[\begin{bmatrix} X \\ Y \\ Z \end{bmatrix}_{\substack{ground\\control}} - \begin{bmatrix} X \\ Y \\ Z \end{bmatrix}_{\substack{aircraft\\position}} \right]$$

For simplicity, the subscript "laser range components" is omitted in the following derivation. Therefore, equation (A-3) can be represented as:

$$\begin{bmatrix} X_1 \\ Y_1 \\ Z_1 \end{bmatrix} = \begin{bmatrix} 1 & -\kappa & \phi \\ \kappa & 1 & -\omega \\ -\phi & \omega & 1 \end{bmatrix} \cdot \begin{bmatrix} l_X \\ l_Y \\ l_Z \end{bmatrix} = \begin{bmatrix} 0 & l_Z & -l_Y \\ -l_Z & 0 & l_X \\ l_Y & -l_X & 0 \end{bmatrix} \cdot \begin{bmatrix} \omega \\ \phi \\ \kappa \end{bmatrix} + \begin{bmatrix} l_X \\ l_Y \\ l_Z \end{bmatrix} \qquad \text{(A-4)}$$

Finally the observation equation becomes:

$$\begin{bmatrix} X_2 \\ Y_2 \\ Z_2 \end{bmatrix} = \begin{bmatrix} 0 & l_Z & -l_Y \\ -l_Z & 0 & l_X \\ l_Y & -l_X & 0 \end{bmatrix} \cdot \begin{bmatrix} \omega \\ \phi \\ \kappa \end{bmatrix} \qquad \text{(A-5)}$$

where:

$$\begin{bmatrix} X_2 \\ Y_2 \\ Z_2 \end{bmatrix} = \begin{bmatrix} X_1 \\ Y_1 \\ Z_1 \end{bmatrix} - \begin{bmatrix} l_X \\ l_Y \\ l_Z \end{bmatrix}$$

For one control point, the observation equation can be established as Equation A-5. For *n* control points, the observation equation will be:

$$B_{3n,1} = A_{3n,3} X_{3,1} \qquad \text{(A-6)}$$

The least squares solution is:

$$\begin{bmatrix} \omega \\ \phi \\ \kappa \end{bmatrix} = X = \left(A^T A\right)^{-1} \cdot (A^T B) \qquad \text{(A-7)}$$

Since the observation is linear, no iteration and initial approximation are needed for the least-squares adjustment. However, if the average positions of tie points are used as control points, iteration is needed to update the average positions of the tie points (Morin and El-sheimy, 2002).

$$\begin{bmatrix} X \\ Y \\ Z \end{bmatrix}_{\substack{average \\ tiepoint}} = \begin{bmatrix} X \\ Y \\ Z \end{bmatrix}_{\substack{aircraft \\ position}} + R_{\substack{body \\ frame \\ to \\ ground \\ rotation}} \cdot R_{misalignment} \begin{bmatrix} l_x \\ l_y \\ l_z \end{bmatrix}_{\substack{laser \\ range \\ components}} \qquad \text{(A-8)}$$

where:

$$\begin{bmatrix} X \\ Y \\ Z \end{bmatrix}_{\substack{average \\ tiepoint}} = (\frac{1}{n}) \begin{bmatrix} \sum X_{tiepoint} \\ \sum Y_{tiepoint} \\ \sum Z_{tiepoint} \end{bmatrix}$$

where:

n : the number of points used to parameterize the tie point

The model must be iterated so that the average constraints are updated for each correction of the calibration parameters. The proposed model addresses the need for true observations by incorporating the tie point interpolation within the adjustment model. The methodology begins by searching for the nearest true observations of the collected tie point within the ALS dataset (Morin and El-sheimy, 2002; Leica, 2003a). The tie point is then parameterized as a function of distances from the nearest true points, i.e.:

$$\begin{bmatrix} X \\ Y \\ Z \end{bmatrix}_{tiepoint} = (\frac{1}{n}) \begin{bmatrix} \sum X_{observed} + dx \\ \sum Y_{observed} + dy \\ \sum Z_{observed} + dz \end{bmatrix} \qquad \text{(A-9)}$$

where:

dx, dy, dz : the initial distances between the measured tie point and the uncorrected, observed ALS ground point.

$(X,Y,Z)_{observed}$: the updated ALS ground points using Equation (A-8)

The averages can be simple averages or weighted by the inverse of distances. The observation equation for the adjustment is then derived as:

$$\begin{bmatrix} X \\ Y \\ Z \end{bmatrix}_{\substack{average \\ tiepoint}} = (\frac{1}{n})\sum_{i=0}^{n}(\begin{bmatrix} X \\ Y \\ Z \end{bmatrix}_{\substack{aircraft \\ position}} + R_{\substack{body \\ frame \\ to \\ ground \\ rotation}} \cdot R_{misalignment} \begin{bmatrix} l_x \\ l_y \\ l_z \end{bmatrix}_{\substack{laser \\ range \\ components}} + \begin{bmatrix} dx \\ dy \\ dz \end{bmatrix}_{\substack{tiepoint \\ distance}}) \qquad \text{(A-10)}$$

Although a single tie point observation equation now contains several ALS observations, they are a linear combination and the partial derivates for the design matrices which are just the weighted average of the partial derivatives for each observation.

Correspondingly, from Equation (A-10), it can be derived:

$$\begin{bmatrix} X_1 \\ Y_1 \\ Z_1 \end{bmatrix} = \frac{1}{n}\sum_{0}^{n}\left[\begin{bmatrix} 1 & -\kappa & \phi \\ \kappa & 1 & -\omega \\ -\phi & \omega & 1 \end{bmatrix}\begin{bmatrix} l_X \\ l_Y \\ l_Z \end{bmatrix}_{\substack{laser \\ range \\ components}}\right] \qquad \text{(A-11)}$$

where:

$$\begin{bmatrix} X_1 \\ Y_1 \\ Z_1 \end{bmatrix} = R^T_{\substack{body \\ frame \\ to \\ ground \\ rotation}}\left[\begin{bmatrix} X \\ Y \\ Z \end{bmatrix}_{\substack{average \\ tiepoint}} - \frac{1}{n}\sum_{0}^{n}\begin{bmatrix} X \\ Y \\ Z \end{bmatrix}_{\substack{aircraft \\ position}} - \frac{1}{n}\sum_{0}^{n}\begin{bmatrix} dX \\ dY \\ dZ \end{bmatrix}_{\substack{tiepoint \\ distances}}\right]$$

Further derivation gives the observation equation:

$$\begin{bmatrix} X_2 \\ Y_2 \\ Z_2 \end{bmatrix} = \begin{bmatrix} 0 & \frac{1}{n}\sum_{0}^{n} l_Z & -\frac{1}{n}\sum_{0}^{n} l_Y \\ -\frac{1}{n}\sum_{0}^{n} l_Z & 0 & \frac{1}{n}\sum_{0}^{n} l_X \\ \frac{1}{n}\sum_{0}^{n} l_Y & -\frac{1}{n}\sum_{0}^{n} l_X & 0 \end{bmatrix}\begin{bmatrix} \omega \\ \phi \\ \kappa \end{bmatrix} \qquad \text{(A-12)}$$

where:

$$\begin{bmatrix} X_2 \\ Y_2 \\ Z_2 \end{bmatrix} = \begin{bmatrix} X_1 \\ Y_1 \\ Z_1 \end{bmatrix} - \frac{1}{n}\sum_{0}^{n}\begin{bmatrix} l_X \\ l_Y \\ l_Z \end{bmatrix}$$

The Equation A-12 is then be used as the observation equation for taking the average of the matched tie points as control points. After getting ($\omega_0, \phi_0, \kappa_0$) for each strip from the first iteration, it is necessary to update the 3-D position of tie points and average them to obtain new control points for next iterating computation until a solution has converged.

1896

Appendix B: Height statistics for two test sites

Table B.1: Height statistics for *SI*

Strip No	Z_mean(m)	Z_std(m)	Z_min(m)	Z_max(m)	Avg. Density (pts/m^2)
1	80.032	47.539	-32.39	256.62	0.534
2	81.871	51.512	28.37	265.55	0.536
3	83.175	49.676	32.24	265.37	0.533
4	82.465	42.936	-1289.52	263.7	0.467
5	83.999	36.749	40.79	253.06	0.493
6	83.291	29.006	40.05	213.9	0.502
7	82.14	21.421	31.33	191.58	0.533
8	92.217	25.446	16.09	217.92	0.532
9	98.889	28.157	6.39	219.21	0.534
10	100.316	21.174	49.16	200.02	0.499
11	106.23	22.51	62.98	200.65	0.409
12	113.197	23.987	21.88	216.38	0.493
13	118.089	23.566	53.22	194.97	0.35
14	122.82	21.688	53.88	209.31	0.412
15	124.592	22.594	53.25	211.31	0.468
16	122.842	24.919	44.25	234.3	0.499
17	119.426	27.202	54.86	234.17	0.464
18	116.974	30.519	50.19	234.1	0.509
19	118.16	31.403	53.26	217.39	0.513

Table B.2: Height statistics for *SII*

Strip No	Z_mean(m)	Z_std(m)	Z_min(m)	Z_max(m)	Avg. Density (pts/m^2)
1	52.269	5.105	-93.680	102.420	0.89
2	53.182	5.050	-92.710	106.150	0.93
3	53.342	4.980	40.200	113.330	0.92

Appendix C: Height differences between laser scanning data and GCPs

Table C.1: Height difference for *SI*

Strips_no	Mean(m)	σ (m)	Min.(m)	Max.(m)	Points No.
1	-0.018	0.117	-0.158	0.119	6
2	0.074	0.084	-0.021	0.137	3
3	0.116	0.049	0.069	0.177	4
4	0.105	0.128	-0.109	0.22	5
5	-0.022	0.163	-0.309	0.25	10
6	0.076	0.132	-0.059	0.228	6
7	-0.052	0.034	-0.109	0.021	9
8	-0.227	0.384	-0.834	0.12	6
9	-0.102	0.416	-0.894	1.033	16
10	-1.569	0.601	-1.877	0.316	12
11	-1.744	0.095	-1.853	-1.604	11
12	-2.063	0.275	-2.351	-1.378	21
13	-1.498	0.67	-1.981	0.967	17
14	-1.687	0.253	-2.151	-1.417	7
15	-1.892	0.228	-2.411	-1.616	8
16	-1.439	0.399	-1.756	-0.859	4
17	-2.043	0.052	-2.079	-2.006	3
18	-1.416	0.655	-1.879	-0.953	3
19	-0.543	N/A*	-0.543	-0.543	1
Min.	-2.063	0.034	-2.411	-2.006	
Max.	0.116	0.67	0.069	1.033	

*Only one GCP falls in the extent of the 19th laser strip data.

Table C.2: Height difference for *SII*

Strips_no	Mean(m)	σ (m)	Min.(m)	Max.(m)	Points No.
1	0.330	0.026	0.272	0.356	9*
2	-0.132	0.046	-0.194	-0.035	9
3	0.124	0.120	-0.156	0.234	12

*The total number of GCPs in test site *II* is 105.

Appendix D: Correspondences from image matching vs. ICP Registration

Correspondences between overlapping strips of airborne LiDAR serve as the input data for strip adjustment computation which estimates and recovers systematic errors. In this dissertation, two methodologies are used to create the correspondence between patches of laser points: (i) *image matching* for boresight calibration; and (ii) *ICP registration* for systematic error validation. Can the matched tie points from overlapping strips via *image matching* techniques be used as corresponding points for systematic error validation? Or, is it possible that the correspondences from *ICP registration* used as tie points for boresight calibration? The experimental results of these two issues will be presented in next two sections.

D.1 Applying the matched tie points using *image matching* as the corresponding points for 3-D similarity transformation

Following the procedures on boresight calibration presented in Section 5.1, the tie points from thirteen patches of *SII* can form the correspondence as the input data for the 3-D similarity transformation by using *image matching* from overlapping patches. The grid size is 0.6 m for interpolation since the average point density is about 2.2 pts/m^2.

Table D.1: The computed seven parameters for *SII*—from image matching (height)

Parameters	Scale (λ)	Ω (deg)	Φ (deg)	K (deg)	t_x (m)	t_y (m)	t_z (m)
Value	0.999938	0.0001224	-0.000464	-0.0000105	-0.523	0.046	-0.553

Table D.2: The computed seven parameters for *SII* — from ICP registration

Parameters	Scale (λ)	Ω (deg)	Φ (deg)	K (deg)	t_x (m)	t_y (m)	t_z (m)
Value	0.999985	0.000428	-0.00777	0.0004968	-0.299	0.302	-0.468

Table D.3: Comparison of planimetric/height differences for strip 1 of *SII*—height

Method	ICP registration			Image matching (height)		
Planimetry/Height	X	Y	Z	X	Y	Z
Average (m)	-0.279	0.290	-0.437	-0.455	0.217	-0.101
Std dev (m)	0.020	0.034	0.025	0.009	0.010	0.066
Min. (m)	-0.317	0.230	-0.488	-0.468	0.196	-0.207
Max. (m)	-0.239	0.352	-0.370	-0.427	0.238	-0.066

Both of the height and intensity images are also used in is section. The results (i.e. described in section 5.3.2 and presented as Table D.2) from ICP registration are used as reference data. For height images, the planimetric and height difference between original and recovered strip 1 are shown in Table D.3 by applying the computed parameters in Table D.1. The difference between two methodologies is significant for both of average planimetric and height differences (Table D.3).

For intensity images, the planimetric and height difference between original and recovered strip are shown in Table D.5 by using the computed parameters in Table D.4. Once again, the differences on the average height/planimetric discrepancy are also significant as Table D.5 shows.

Table D.4: The computed seven parameters for *SII*—from image matching (intensity)

Parameters	Scale (λ)	Ω (deg)	Φ (deg)	K (deg)	t_x (m)	t_y (m)	t_z (m)
Value	1.000252	-0.0001563	-0.003397	0.0000542	-0.328	0.428	-1.088

Table D.5: Comparison of planimetric/height differences for strip 1 of *SII*—intensity

Method	ICP matching			Image matching (intensity)		
Planimetry/Height	X	Y	Z	X	Y	Z
Average (m)	-0.279	0.290	-0.437	-0.382	-0.244	-0.582
Std dev (m)	0.020	0.034	0.025	0.036	0.043	0.457
Min. (m)	-0.317	0.230	-0.488	-0.474	-0.330	-1.206
Max. (m)	-0.239	0.352	-0.370	-0.289	-0.154	0.417

It is concluded that the interpolation of laser points to a regular grid will reduce the accuracy of the parameters from the 3-D similarity transformation. In addition, it reveals that the interpolation should be avoided while validating the systematic errors for laser point clouds.

D.2. Applying the corresponding points using *ICP registration* as the tie points for boresight calibration

The four boresight test strips used in the section 5.1 are also used in this section. Correspondingly, the first strip is fixed while applying the ICP registration. The difference between the initial and calibrated tie point are depicted in Tables D.6 and D.7, respectively.

Table D.6: Initial tie point differences

	X (m)	Y (m)	Z (m)
Mean	0.416	0.566	12.999
Median	0.426	0.584	12.653
Minimum	0.244	0.386	9.359
Maximum	0.567	0.764	16.174
Std Dev	0.119	0.134	2.281

Table D.7: Tie point differences after calibrated

	X (m)	Y (m)	Z (m)
Mean	26.996	20.461	5.209
Median	27.271	20.450	5.387
Minimum	13.570	19.450	0.547
Maximum	30.786	23.846	7.769
Std Dev	1.822	0.759	1.661

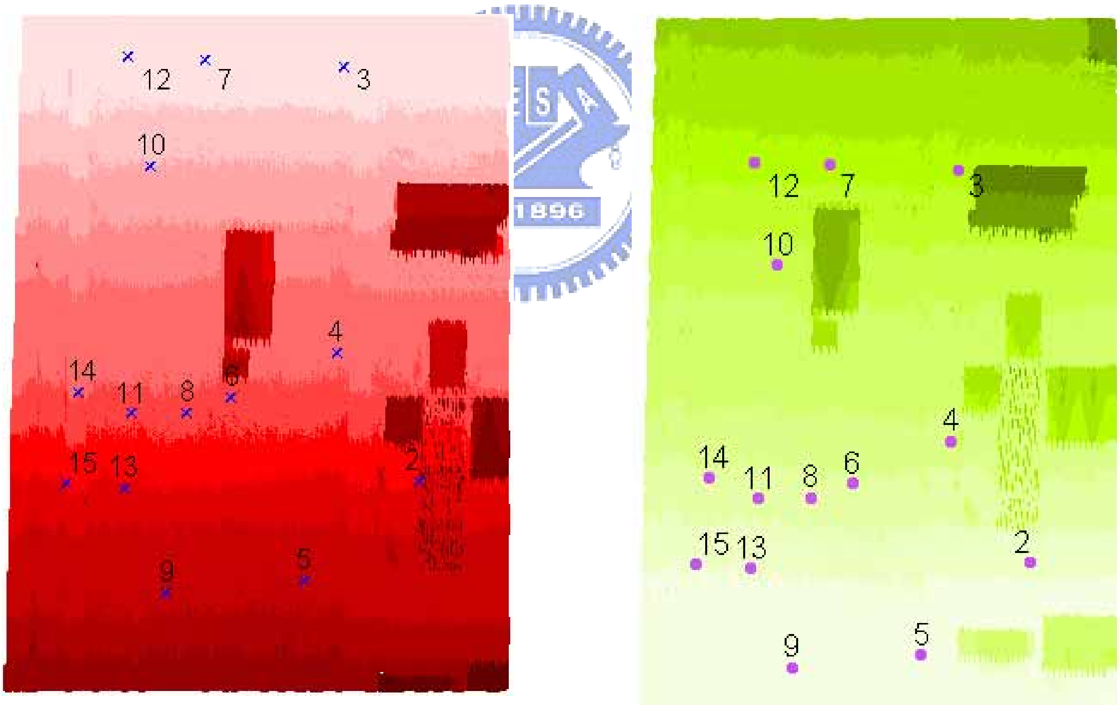

Figure D.1: Mismatched tie point from ICP registration

One of the interesting things in Tables D.6 and D.7 is that the calibrated tie point difference is much larger than the initial tie point difference. The principle of the *ICP algorithm* establishes correspondences between data sets by matching points in one data set to the closest points in the other data set. Therefore, the Euclidean distance between data sets will play a key factor to search the corresponding points. As Figure D.1 shows, the mismatched tie points are selected since they were found under the searching distance criteria.

The calibrated boresight parameters are presented as Table D.8. Compared to the boresight parameters which derived from manual selection on intensity images (Table 5.3), the boresight misalignment angles are apparently not well-calibrated though their angular accuracy is much better than the accuracy of IMU (0.005 degrees for roll and pitch, 0.008 for heading).

Table D.8: Boresight parameters from ICP matching

Parameters	Value	Standard deviation	Standard deviation
Roll Error	-0.02616208 rad	0.00001258 rad	0.0007206 degrees
Pitch Error	0.00012800 rad	0.00001978 rad	0.0011336 degrees
Heading Error	-0.02206980 rad	0.00007932 rad	0.0045446 degrees
Torsion	-1117.656 units	0.4628088 units	0.4628088 units

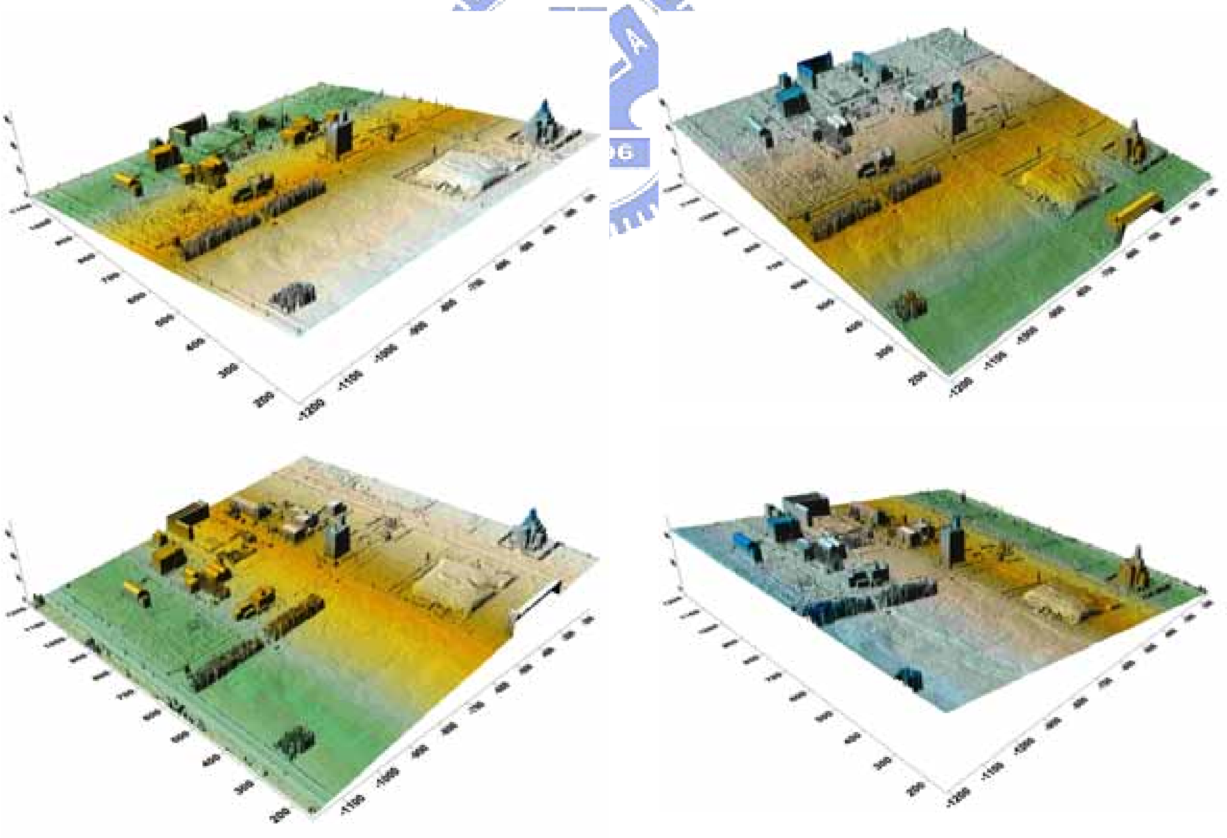

Figure D.2: The strips are distorted across all 3 dimensions.

Due to the intentional incorrect misalignment angles given for boresight calibration in four testing strips, the position of tie points are affected by the large planimetric shifts (Figure D.2). Thus a grid point in one strip will generally not correspond to the same point in the others. To apply the *ICP registration* to select the tie point for boresight calibration, it is necessary to acknowledge the disadvantages of *ICP algorithm*.

The disadvantage for the *ICP algorithm* is that the correct registration is not guaranteed, since (i) it may fall into wrong local minima, and (ii) it requires approximate registration. A few possible ways to generate more reliable solutions on boresight calibration with the tie points from ICP registration are: (i) applying the initial boresight parameters on uncalibrated strips that ALS system provided to have better approximation, and/or (ii) using a dynamic distance threshold on the distance allowed between closest points (Zhang, 1996) or adding some control points (Chen and Medioni, 1991).

VITA

June 7, 1967 .... Born –Hsinchu, Taiwan

July 1989 .... BSc. Survey and Mapping Engineering
Chung-Cheng Institute of Technology
Tao-Yuan, Taiwan

September 1998 .... MSc. Geodetic Science and Surveying
The Ohio State University, Columbus, Ohio, USA

2001-2005…………………………………………….. Graduate Research Assistant,
National Chiao Tung University, Hsinchu, Taiwan

Publication List

Refereed Journal Publications:

1. Shih, T. Y. and Liu, Jung-Kuan, 2005. Effects of JPEG2000 Compression on Automated DSM Extraction: Evidence from Aerial Photographs, Submitted to *Photogrammetric Record*, 20(112):351-365.（SCI）
2. Liu, Jung-kuan, H. C. Wu, and T. Y. Shih, 2005. Effects of JPEG2000 on the Information and Geometry Content of Aerial Photo Compression, *Photogrammetric Record & Remote Sensing*, 71(2):157-168.（SCI）
3. Li, Rongxing, Jung-kuan Liu, Yaron Felus, 2001. Spatial Modeling and Analysis for Shoreline Change Detection and Coastal Erosion Monitoring, *Marine Geodesy*, Vol. 24, No. 1, pp.1-12. (SCI Expanded)
4. Liu, Jung-kuan, W. C. Hsu, T. Y. Shih, and J. K. Liu, 2005. A Preliminary Study on the System Calibration of An Airborne Lidar System, *Journal of Surveying Engineering*, Vol. 47, No. 2, pp.49-66 (In Chinese).
5. Wu, W. C., T. Y. Shih, and Jung-kuan Liu, 2005. The Comparison of Three Wavelet Based Image Compression Implementation, *Journal of Photogrammetry and Remote Sensing*, Vol. 10, No. 3, pp.305-314 (In Chinese).
6. Liu, Jung-kuan, 2000. An Application of Dynamically Segmented Linear Data Model, *Transaction on Surveying & Optical Technology*, Vol. 102, pp.59-69 (In Chinese).
7. Liu, Jung-kuan, 1999. Developing Geographic Information System Applications in Analysis of Responses to Lake Erie Shoreline Changes, *Transaction on Surveying & Optical Technology*, Vol. 101, pp.93-106 (In Chinese).
8. Liu, Jung-kuan, 1996. Study on Facility Management System in Military Base, *Journal of Corps of Engineers*, Vol.100, pp.53-64 (In Chinese).

Papers Submitted for Refereed Publications:

1. Jung-Kung Liu, Rongxing Li, Tian-Yuan Shih, 2005. Estimation of Bluffline by Integrating Topographic LIDAR Data and Orthoimages, Submitted to *ISPRS Journal of Photogrammetry and Remote Sensing*. (SCI)

Conferences Papers:

1. Li, R., J.-K. Liu, X. Niu, and T.-Y. Shih, 2005. On the integration of Airborne Lidar data and orthoimages for Bluffline Mapping, the *25th IGARSS*, Korea.
2. Liu, Jung-kuan, W. C. Hsu, and T. Y. Shih, 2005. A Preliminary Study on the System Calibration of An Airborne Lidar System, *24th Surveying Engineering and Applications Conference*, Taipei, Taiwan, Sep. 8-9.
3. Shih, T. Y., J.-K. Liu, 2003. The Effects of JPEG2000 Compression on Automated DTM Generation, *Asian Conference on Remote Sensing*, Busan, Korea, Nov. 3-7.
4. Shih, T. Y., J.-K. Liu, Y. H. Tseng, 2003. On the Comparisons of Accuracy of Elevation on Airborne Lidar and DTM from Automated Generation, *22th Surveying Engineering and Applications Conference*, Tachi, Taiwan, Sep. 15-16.
5. Shih, T. Y., J.-K. Liu, H. C. Wu, 2002. On the Performance of JPEG2000 for Aerial Photo Compression, *Asian Conference on Remote Sensing, Kathmandu*, Nepal, Nov. pp.25-29.
6. Liu, Jung-kuan, 2000. Managing Spatial Data with Minimum Spanning Tree – A Java Applet, *19th Surveying Engineering and Applications Conference*, ChangHwa, Taiwan.
7. Liu, Jung-kuan, 2000. A Workflow for Joint Operations Graphic with Digital to Plate System, *Annual Conference for Surveying & Optical Engineering*, Topographic Service, TaiChung, Taiwan.
8. Li, R., J.-K. Liu and Y. Felus 1999. Spatial Modeling and Analysis for Shoreline Change Detection and Coastal Erosion Monitoring. *Geoinformatics 99*, Ann Arbor, MI, June 19-21.
9. Li, R., G. Zhou, A. Gonzalez, J.-K. Liu, F. Ma, Y. Felus, M. Lockwood, G. Tuell, N. Schmidt and C. Fowler 1999. Shoreline Mapping and Change Monitoring Using High-Resolution Airborne and Satellite Imagery. Poster at *GeoTools 99*, Charleston, SC, April 5-7.
10. Liu, Jung-kuan, R. Li, 1999. Quantify and Display Shoreline Change – An Alternative Way, *18th Surveying Engineering and Applications Conference*, YiLan, Taiwan.

Others:

1. Liu, Jung-kuan, 2000. Operation Manual of Digital to Plate System – NT Version, Topographic Service, Combined Service Forces, Taiwan, (In Chinese).
2. Li, R., Zhou, G., Gonzalez, A., Liu, J-K, Ma, F. and Felus, Y., 1998. Coastline Mapping and Change Detection Using One-Meter Resolution Satellite Imagery, Annual Project Report, The Ohio State University, Columbus.
3. Liu, Jung-kuan, 1998. *Developing Geographic Information System Applications in Analysis of Response to Lake Erie Shoreline Changes*, Master's Thesis, The Ohio State University, Columbus.

Fields of Study

Major Field: Geodetic Science